Investigating Boosted Decision Trees as a Guide for Inertial Confinement Fusion Design

Andrew D. Maris[1,2], Shahab F. Khan[1,a)], Michael M. Pokornik[1,3], J. Luc Peterson[1], Kelli D. Humbird[1], Steven W. Haan[1]

[1]Lawrence Livermore National Laboratory, Livermore, CA, USA, 94550
[2]Massachusetts Institute of Technology, Cambridge, MA, USA, 02139
[3]University of California San Diego, San Diego, CA, USA, 92093
[a)]Author to whom correspondence should be addressed: khan9@llnl.gov

Abstract:

Inertially confined fusion experiments at the National Ignition Facility have recently entered a new regime approaching ignition. Improved modelling and exploration of the experimental parameter space were essential to deepening our understanding of the mechanisms that degrade and amplify the neutron yield. The growing prevalence of machine learning in fusion studies opens a new avenue for investigation. In this paper, we have applied the Gradient Boosted Decision Tree (GBDT) machine learning architecture to further explore the parameter space and find correlations with the neutron yield, a key performance indicator. We find reasonable agreement between the measured and predicted yield, with a mean absolute percentage error on a randomly assigned test set of 35.5%. This model finds the characteristics of the laser pulse to be the most influential in prediction, as well as the hohlraum laser entrance hole diameter and an enhanced capsule fabrication technique. We used the trained model to scan over the design space of experiments from three different campaigns to evaluate the potential of this technique to provide design changes that could improve the resulting neutron yield. While this data-driven model cannot predict ignition without examples of ignited shots in the training set, it can be used to indicate that an unseen shot design will at least be in the upper range of previously observed neutron yields.

1. Introduction

Inertial confinement fusion (ICF) experiments at the National Ignition Facility (NIF) [1] have recently set fusion energy yield[2] records across ICF platforms. This was accomplished with NIF's unique capability of producing 2MJ of laser energy with 192 individual beamlines. In an indirect drive experiment, NIF's ultraviolet beams irradiate the inside of a gold or uranium coated cylindrical cavity known as a hohlraum, creating a near-uniform X-ray environment [3]. The X-ray bath drives a spherical implosion of a small DT capsule suspended in the middle of the hohlraum by ablating the capsule's outer layer of high-density carbon or other material. After the laser pulse is turned off, the remaining shell material continues moving spherically inward at a rapid pace via conservation of momentum. This radial kinetic energy compresses and heats the gaseous fuel in the center of the capsule to the pressures and temperatures required for fusion to occur. During the < 100ps timeframe of maximum compression, DT fusion begins at the central hotspot, triggering a burn wave that propagates through the compressed capsule.

In 10+ years of NIF operations, it has proved challenging to create symmetric and efficient implosions. Many experimental configurations have been tried across a wide parameter space that includes the shape and size of the hohlraum, the engineering design of the capsule (such as the radius, fill tube size), and the power and duration of each part of the laser pulse, among other factors. Several of these design parameters are illustrated in Fig. 1. The laser pulse shape, as shown in Fig. 2, has several epochs called the picket, trough, transition, and main pulse (also known as the peak). Each epoch of the pulse has a corresponding amplitude and duration parameter.

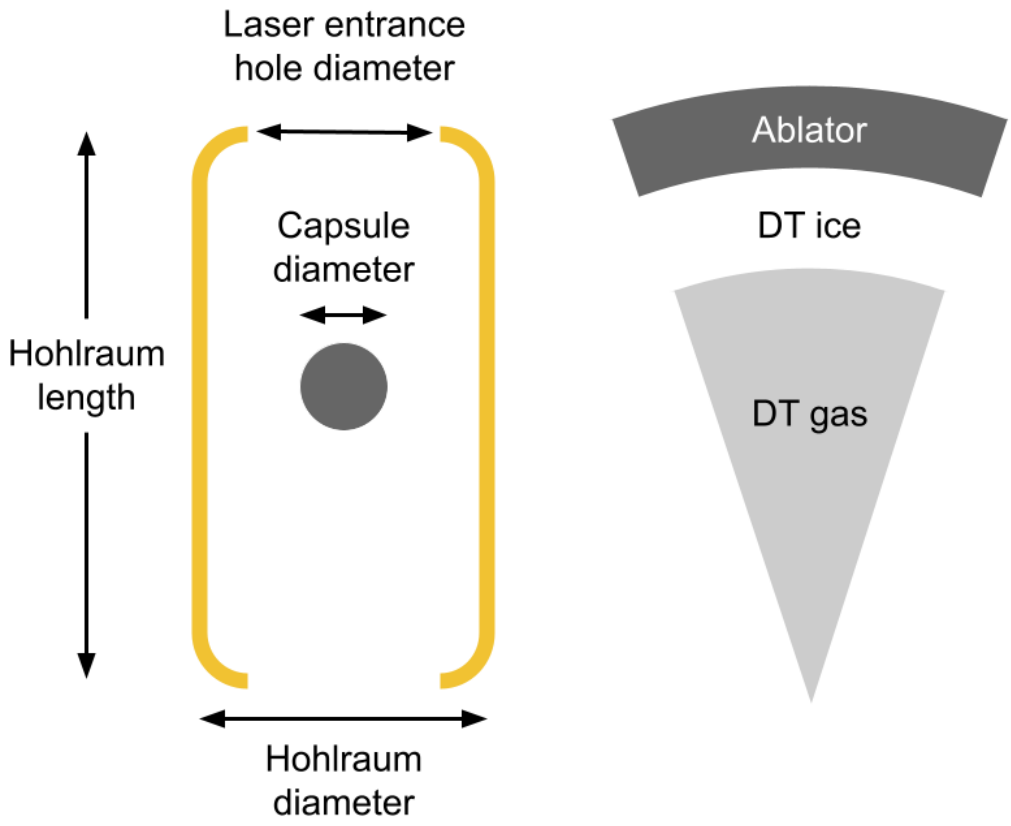

Figure 1: A diagram of a hohlraum and capsule (left) and a triangular cross-section of a DT capsule (right).

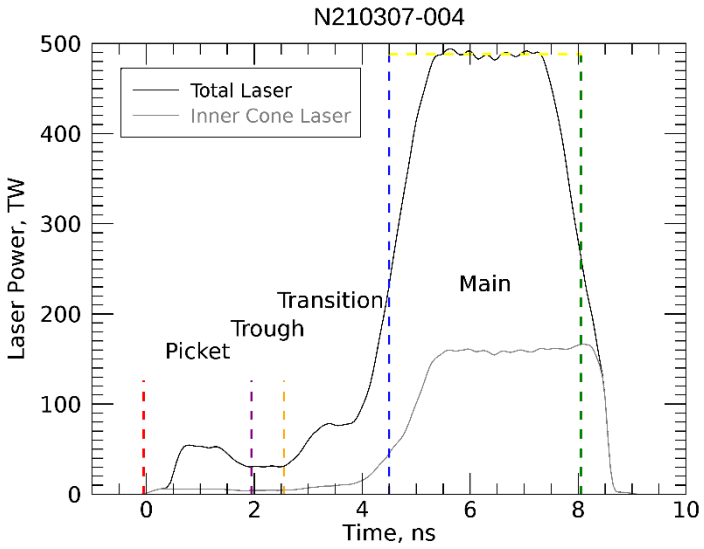

Figure 2: An example of the measured laser pulse shape of shot N210307-004, a shot from the Hybrid-E campaign. The part of the pulse between the red and the purple dashed line is the "picket," between the purple and yellow is the "trough," between the yellow and blue is denoted as the "transition region" and between blue and the green is the "main pulse."

As experiments at NIF have progressed towards higher fusion yields, machine learning (ML) has become an increasingly valuable tool in studies of high-energy density physics (HEDP) and nuclear fusion [4]. These fields provide promising frontiers for ML because of the abundance of experimental and simulation data. ML has been used to develop tokamak disruption prediction systems [5,6], identify a physical computational fidelity boundary for HEDP simulations [7], create more efficient plasma-diverter interaction models relevant to ITER [8], and assist researchers to discover an improved plasma confinement regime [9], among a host of other applications.

ICF experiments at NIF present a unique challenge for ML because of the relatively small number of experiments and the diversity of parameters between shots. To date, there have been fewer than 250 Deuterium-Tritium (DT) ICF shots in NIF's operational history. During that time, experimental parameters of DT shots such as tent thickness, ablator material, and pulse shape have changed considerably with the research community's evolving understanding of ICF physics. The small sample size and heterogenous quality of the NIF data pose obstacles to conventional deep learning techniques which require vast quantities of training data. ICF researchers have generally addressed this problem in the past using simulated data for all or most of the training process, such as efforts that succeeded in tripling the record of direct drive yield at the OMEGA laser facility [10] and approaches led by NIF that delivered insights into the physics of indirect drive [11,12]. ICF simulations, however, do not capture all the details involved in the experiments and can be computationally expensive if considering 3D effects. Including experimental measurements of implosions through transfer learning has shown promise in improving ICF prediction performance [13].

Another branch of work has sought to identify the prediction performance of algorithms trained purely on experimental data at NIF and identify feature importance [14,15]. This paper complements and extends beyond past work by 1) leveraging the Gradient Boosted Decision Tree (GBDT) [16] architecture, 2) utilizing

only shot design & manufacturing parameters to predict the yield, 3) including features related to degradation mechanisms such as DT ice asymmetries, 4) visualizing the performance contours predicted by the model to inform shot design, and 5) focusing only on High Density Carbon (HDC) shots. No diagnostic data about the implosion, such as ion temperature, were used to predict the yield. Our model only makes predictions from information about the shot's design and manufacturing, such as the laser pulse specifications (peak power, trough length, etc.) and target characteristics (fill tube diameter, ice layer asymmetry, etc.). Using this approach allows us to focus our parameter space to a set of capsule design parameters that can be directly controlled. For example, the models could be used to adjust the choice of laser pulse and target specifications to maximize fusion yield. In terms of features related to degradation mechanisms, we include tent thickness and fill tube diameter, as in previous studies, as well as measurements of ice layer quality (such as K number[17] and size of grooves) and whether the improved HDC capsule fabrication technique was employed. We focused only on HDC experiments to reduce the number of variables and to prevent the model from using parameters as a campaign "selector". For example, "Low Foot" experiments with low yield values can be selected by the algorithm by isolating parameters that have a range of values unique to Low Foot experiments, such as long pulse durations. By directing our study at HDC capsule experiments alone, we make our analysis relevant to the highest performing experiments at NIF as well as the current and likely future focus of experimental campaigns. A Pearson Correlation Matrix of all 37 features used in this study can be found in Appendix B.

We find that this machine learning algorithm achieves a mean absolute percentage error (MAPE) of 35.5% on a randomly chosen test set, which is larger but comparable to the observed yield variance of 10-25% for "repeat" shots at NIF [18]. The most important parameters for this model to accurately predict yield include the laser pulse picket cone-fraction[19], the laser peak duration, the laser energy, the hohlraum laser entrance hole (LEH) diameter, and the capsule quality (flag). The laser peak duration, laser energy and LEH are directly related to the laser drive and ablation pressure. The model finds that the capsule quality is of secondary importance. Further, parameters that were otherwise thought of as important are shown to have a lower influence in this model (partly because it focuses on the HDC subset of shots) such as the laser picket strength and the K number (the DT ice layer non-uniformity factor). We performed a design space scan of several experiments including shot N210808[20–22], the first experiment to exceed 1MJ of fusion yield.

2. Methods

Our data set comprises of 77 DT ICF shots that use the HDC ablator starting with shot N160223 and ending with N221107. The campaigns in the study include the original "HDC"[23–25], "BigFoot"[26–28], Hybrid-B[29], Hybrid-E[30,31], I-raum[32], and SQ-n (Scaling Quality)[33] designs. Certain shots were excluded because they were specifically designed for some purpose other than DT compression and burn, and those with known experimental irregularities such as a defective laser bundle (quad) or aged DT fuel[34].

The 37 input features (see Pearson Correlation Matrix in Appendix B) include shot design parameters such as ablator thickness and physics-informed composite metrics such as the case to capsule ratio (the ratio of the hohlraum diameter to capsule diameter). We include a broad set of parameters known or suspected by the community to influence ICF yield, significantly more than utilized in past applications of machine learning to NIF experiments. It should be noted that capsule quality information, thought to be one of the primary degradation mechanisms[35,36], is not consistently available across these shots. An

enhanced fabrication technique that reduces the number of pits on the capsule surface was used on most DT shots after N210808. To account for this discontinuous improvement, we include a capsule quality proxy variable that is 0 for experiments using the previous fabrication method and 1 otherwise.

We investigated whether a smaller set of features would improve prediction performance through 1) dimensionality reduction techniques such as PCA and Factor Analysis of Mixed Data (FAMD), 2) explicit feature selection during the cross-validation stage, and 3) manually dropping features expected to be insignificant. In all cases, the prediction performance was worse or not significantly better than the case where all features were used. This is consistent with the implicit feature selection that occurs during the training of tree-based algorithm. In most of the paper, we report the results when trained on all 37 features, however similar performance can be obtained by using 10-20 features. The output of our models is the base 10 logarithm of the neutron yield.

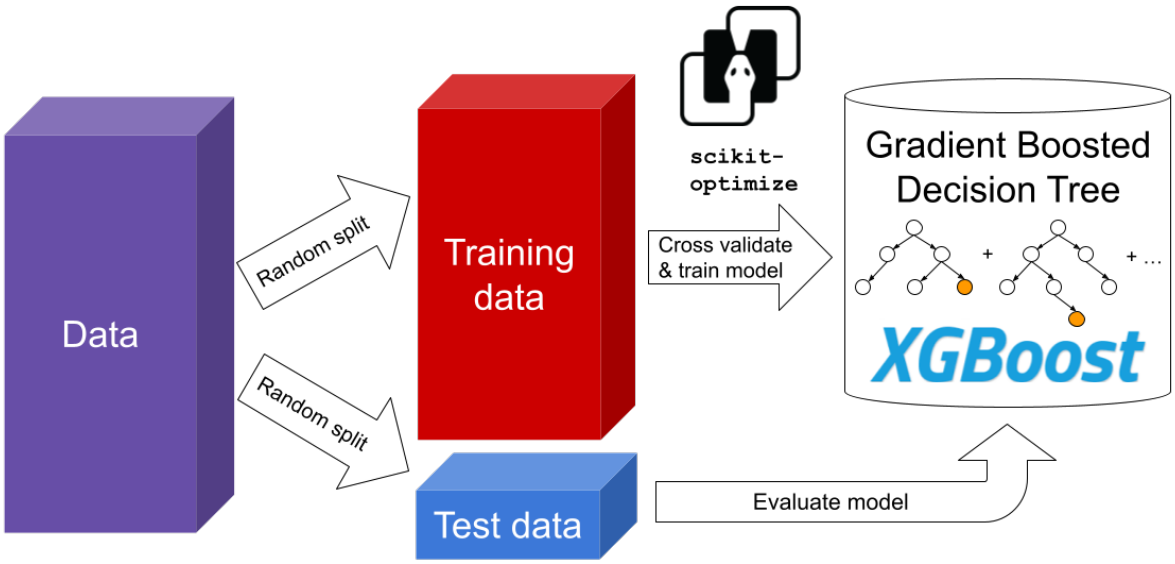

Figure 3: A diagram of the machine learning pipeline utilized in this project. We split the data into training (80%) and test (20%) sets. We use the scikit-optimize package on the training data to determine the best hyperparameters. We evaluate the model by measuring the accuracy of predicting the yield on the test data.

A diagram of the machine learning pipeline is shown in Figure 3. We train GBDTs using the software package XGBoost [37], which has been successful in other physics-related tasks [38]. Additionally, decision tree-type architectures like GBDT are generally favored in settings with a relatively large feature to sample ratio such as this. We automated the hyperparameter search process using the python package scikit-optimize. The model performance during this phase is measured as mean absolute error (MAE) of leave one out cross validation (LOOCV). We use a standard 80/20 train/test split in this study. The DART tree booster, incorporating a tree dropout technique to potentially reduce overfitting, was chosen for the model. The model hyperparameters can be found in appendix A.

An advantage of tree-based ML architectures is their straightforward methods for estimating the relative importance of individual features in models. This endows the model with a level of interpretability that is otherwise challenging or impossible to achieve for black box architectures such as neural networks. For physics-based applications like ICF yield prediction, feature importance metrics can boost confidence that the model is learning physically valid relationships and point to important

correlations to inform theoretical models. In this study, we report the 'Total Gain' feature important metric from the Xgboost package, which estimates the improvement of the prediction caused by including a particular feature across all splits in the model's tree structure.

Using a trained model, we can explore the parameter space to quantify relationships to yield. For example, we can evaluate how the performance reacts to small changes in picket power and trough length (adiabat and shock timing) or peak power and peak duration (coast time) or LEH diameter. To do this, we train the model on all experiments with previously determined hyperparameters and then evaluate the predicted performance of a single experiment as we vary up to two parameters. This allows visualization of the optimal parameters combinations for maximizing yield.

An example of a typical NIF laser pulse with varied picket power and trough length is shown in Figure 4. We developed a script to determine the start, middle, and end of each portion of the laser pulse using derivatives and thresholds. We can then scale the amplitude and/or time to see how the model's predictions are affected by these changes. The model only accepts higher level features, but this scaling script ensures that interdependent parameters are varied correctly (such as trough length and total laser pulse energy). For instance, extending the trough region also increases the total laser pulse energy and the total duration of the laser pulse.

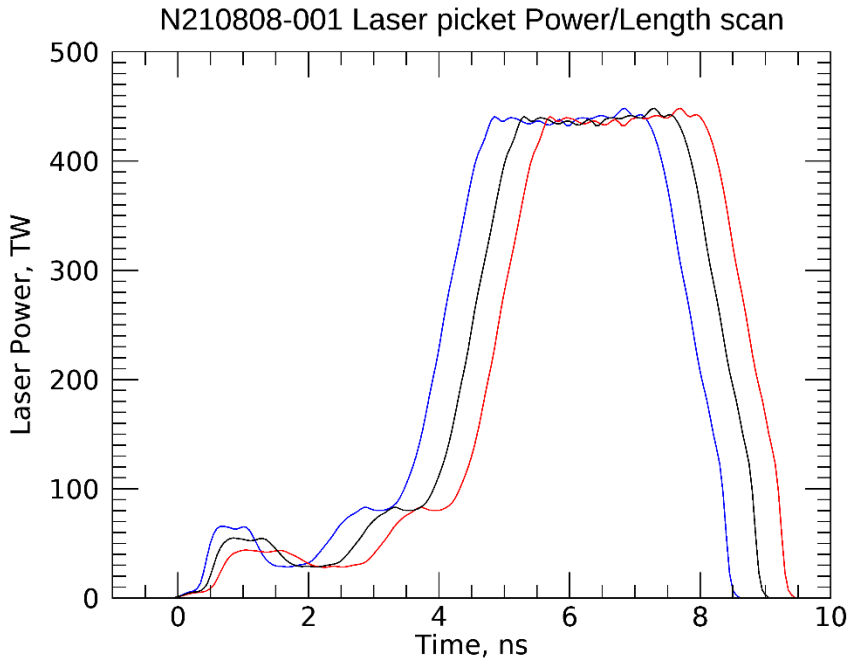

Figure 4: The total laser pulse is altered by stretching/shortening certain epochs in time and/or scaling the amplitude by a multiplicative factor. We use the measured laser pulse (post shot).

3. Results and Discussion

We find that the GBDT model achieves reasonable neutron yield prediction performance. The feature importance metrics indicate that the model relies most heavily on characteristics of the laser drive. We

also test the model on mock experiments that are slight variations of some notable experiments in the Hybrid-E, BigFoot and the SQ-n campaigns. We note that the GBDT model does not extrapolate well to parameter values outside the previously explored experimental design space.

Accuracy

The mean absolute percent error (MAPE) of the predicted yield (Figure 5a) for the randomly chosen test set is 35.5% with a corresponding train set MAPE of 18.8%. This error is comparable to the 10-25% repeatability of neutron yield outputs of identical DT shots at NIF [18]. Compared to the performance of the Random Forest (RF) models for predicting the neutron yield reported by [14], our model achieves a modestly higher test set performance (test R^2 = 0.86, compared to 0.82, 0.80, and 0.74 in the three RF models presented in [14]) with comparable training loss (train R^2 = 0.95, compared to 0.96, and 0.96, and 0.95 [14]). The smaller gap between the training and test accuracy indicates there is a lesser, but still not insignificant, amount of overfitting.

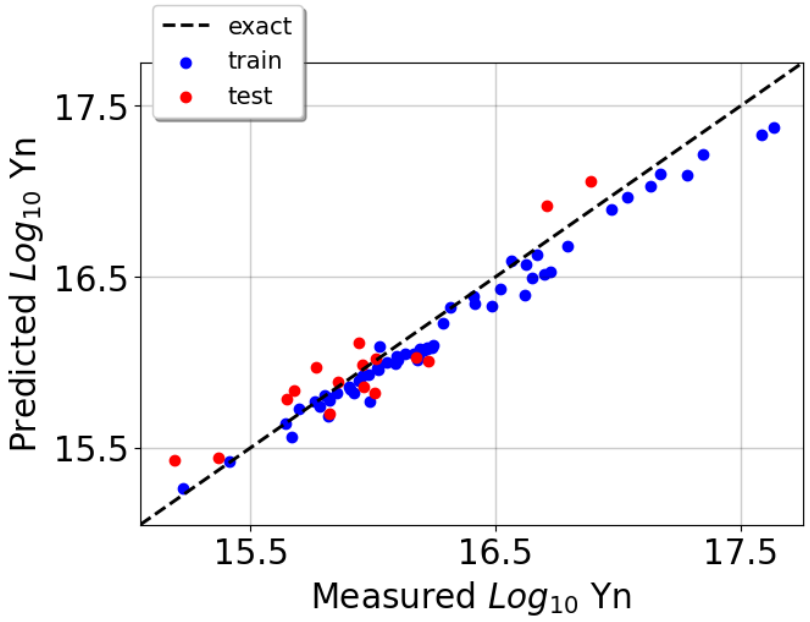

Figure 5: Comparison of predicted yield vs measured yield for a randomly assigned train and test set. Perfect predictions would fall along the dotted line.

Given the tendency of tree-based architectures like GBDT to only make predictions bounded within the range of labels (in this case, the yield) observed in the training set, we expect the model to underpredict future shots with higher yield, such as those that achieve ignition. The discontinuous change in the dominant physics when entering the alpha heating regime are not well captured by the dataset of existing shots. Nevertheless, the model could still be leveraged to indicate that the yield of a particular design will at least be within the upper range of data already observed. In other words, we could use this model to indicate whether we are close to the ignition threshold, even if the model cannot say that we will go past it. Given the nonlinearities of self-heating, there may be little difference between a

design at the threshold and past the threshold of ignition. This model can quickly discriminate low yield shots from high yield shots with a reasonable degree of accuracy.

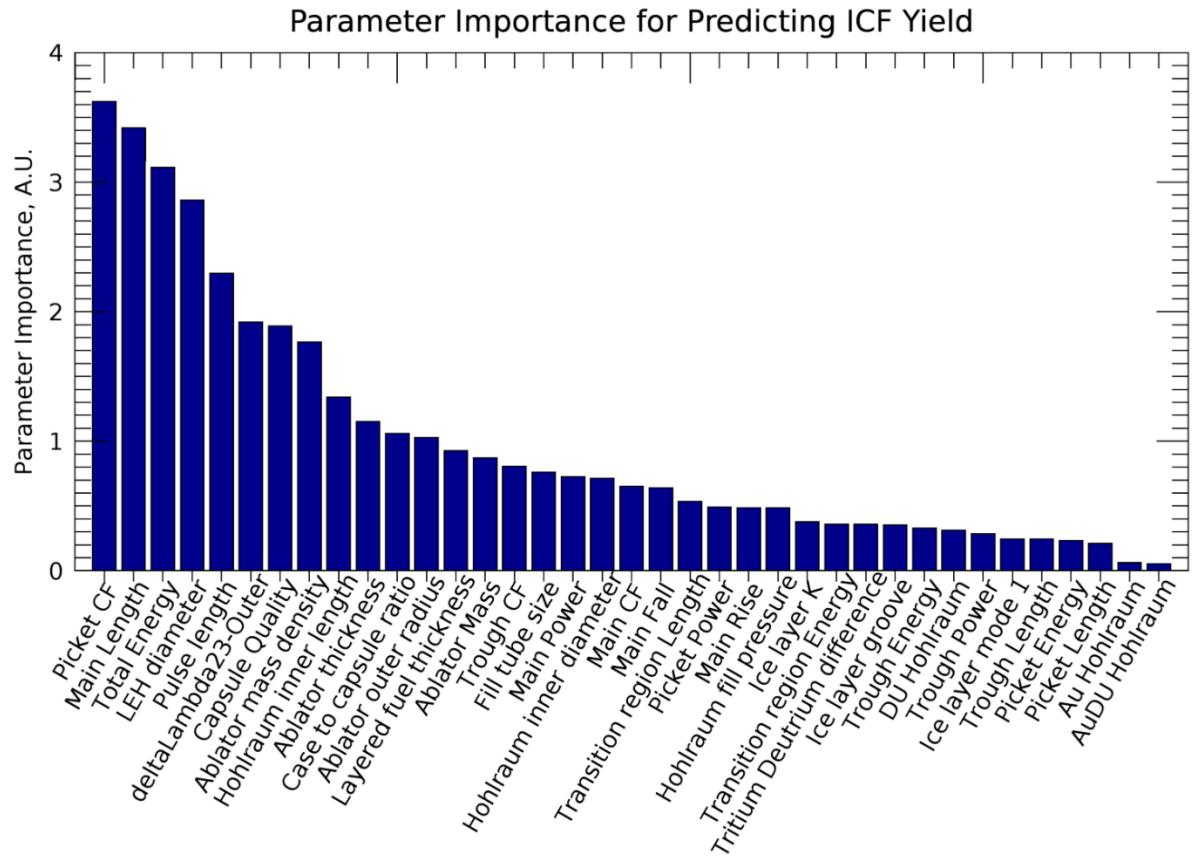

Figure 6: The parameter importance of all the features when the model is trained on all experiments.

As stated earlier, we measured feature importance using the 'Total Gain' metric. Previous studies [14,39] have noted strong correlations exist between features in the NIF dataset, which suggests we must use a degree of caution when interpreting feature importance metrics since the true physically relevant parameters may correlate with less relevant parameters.

We report the feature importance scores (Total Gain) of all the features in Fig. 6, normalized to the mean score across all features. The top eight features mostly relate to the laser pulse characteristics (ex. picket cone fraction, length of main pulse), but also include the laser entrance hole diameter, the capsule quality flag, and the mass density of the ablator. The picket cone fraction (CF) is used to tune the symmetry of the implosion very early in time. However, it is more likely that this parameter is being used as a campaign selector. The Hybrid-E experiments use about 10% CF while the HDC and BigFoot designs use a CF mostly greater than 13%. Further evidence of the CF serving as a campaign selector will be shown during the discussion of the design space scans. The second most important parameter is not much of a surprise: the main length, or duration of the peak, is analogous to "coast-time" which is known to strongly impact to the performance.[40] The total energy and LEH diameter parameters are expected as well, as they control the velocity and time of compression. A smaller LEH diameter leads to

less energy escaping the hohlraum and therefore a higher hohlraum radiation temperature (T_{rad}) to drivie the implosion. High fusion performance would not be possible without a high T_{rad} to provide sufficient drive, regardless of LEH diameter. Another interesting parameter (rank 6) is the λ_2-λ_3 (wavelength difference between the outer and 23° inner beams). The $\Delta\lambda_{23}$ is used to tune the symmetry of the implosion as the wavelength difference induces energy transfer between the beams that cross each other on top of the LEH[41] Indeed, some of the recent higher performing shots used the $\Delta\lambda_{23}$ to tune the symmetry round (tuning done using "sym-caps"[19,24] and 2-D radiography experiments[42]). The seventh most important feature, according to this model, is the capsule quality flag. This flag is 1 for all shots after N210808 except for N220129, which used a capsule from an older batch. This capsule quality flag is set to 0 on all other shots. Ideally, we would want to use variables for the capsule quality that would count the voids and pits with certain sizes. When this data is consistently available, we intend to include it in a future model. It makes sense that this is ranked highly since the improved capsule quality is thought to have played a large role in the recent successes at the NIF.

This feature importance hierarchy is somewhat different from those found in [14], which uses a different decision tree-like architecture, feature importance metric, and includes both plastic and Beryllium ablator experiments in the training and test set. Both approaches place significant emphasis on laser energy, but our model does not rank picket power or main power highly. We think the reason that picket strength (energy or power) is not as important in our study is due to the exclusion of LowFoot experiments. Without the large range of picket strength values with accompanying yields (LowFoot = low yield), the picket strength was deemed a less valuable parameter. However, as will be shown during our discussion of picket power scan, that the picket power does modestly influence performance. One notable similarity with the Random Forest in the previous study [14] is that this GBDT model also placed a large emphasis on $\Delta\lambda_{23}$.

We suggest the reader uses caution when interpreting the feature importance measurements because the limitations of using a single number to quantify the complex influence of a feature in a model. There are strong, nonlinear relationships between the features and the model's predictions that are not fully reflected by a scalar feature importance score. As stated earlier, features are also correlated with one another, which could cause the model to infer importance of a feature that is simply correlated with a physically relevant feature. We suggest the reader interprets the individual feature importance as correlations that are suggestive of physical relevance, but not proof in and of itself.

Sensitivity of performance with number of features

Given the presence of overfitting, one may wonder whether performance on the test set could be improved if the model is trained on fewer features. Figure 7 shows the train and test set MAPE as features are sequentially added to the model in the order of their feature importance Fig. 6. For each step, we re-run the hyperparameter search with 7-fold cross validation to find a suitable set of hyperparameters for each combination of features.

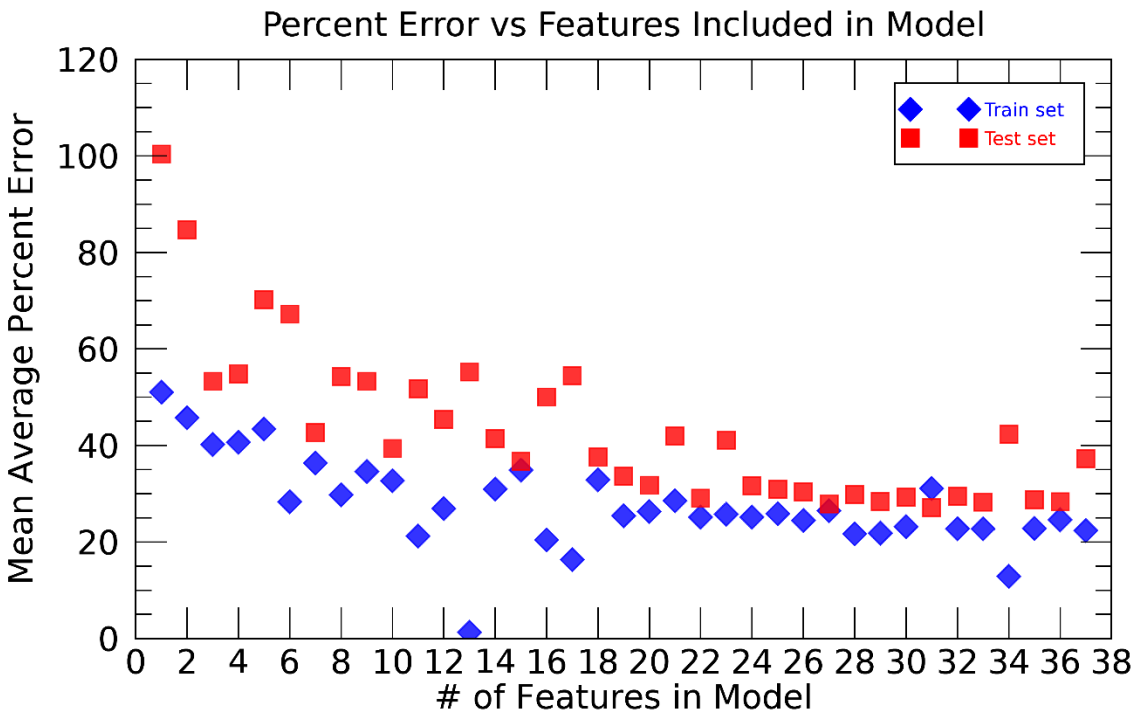

Figure 7: The trend in train and test set error with number of features. Features are sequentially added in order of importance reported in Fig. 6. Test set error and overfitting tends to decrease with number of features until reaching a plateau when >20 features are included in the model.

We find that as the number of features increases, the test and train set errors tend to decrease until reaching a plateau when more than 20 features are included in the model. Beyond that point, the test set error bounces within the range of 25-45% while the train set error generally stays within 20-30%. There tends to be less overfitting beyond >20 features, although overfitting is apparent in that regime, as evidenced by the cases where train error is less than or nearly 20% generally having significantly higher test error (~40%) than other cases (test error: ~30%). The lowest test error across all feature combinations is the case with 31 features, achieving a test error of 27.1% and a training error of 31.1%.

We find that this GBDT approach for predicting yield tends to benefit from a large number of features (>20). Other machine learning architectures, such as neural networks, tend to suffer significant overfitting when there are many features and relatively few samples, but the GBDT model performance in this case is generally robust out to the maximum number of features. More than 20 features may not strictly be necessary to achieve <30% test error, but the model tends to achieve higher performance with >20 features.

Predicting performance with design variations

Coast time and peak power

An advantage of this approach to predicting yield is the rapid predictive capability of performance as a function of shot design and manufacturing conditions. Both training the model and subsequently making thousands of predictions is computationally trivial, allowing us to explore, for example, how the coast

time and peak power can affect the performance of any past or future HDC experiment. In Fig 8a, we show the first exploration of the relative performance relationships with design/manufacturing parameters. In these plots, each point in the 2D maps was computed by predicting the yield of alternate version of the shot using the version of the GBDT model trained on all shots in the dataset. As discussed in the Methods Section, when changing the coast time (peak length) or peak power, other laser parameters such as the total energy and total pulse length are recalculated accordingly. The GBDT model correctly identifies that increasing the energy will generally increase the yield for all three shots. The dashed line represents the 2MJ laser energy contour, which is close to the upper range of laser energy at NIF. Experiments designed to investigate the effect of coast time usually vary the peak power and peak length parallel to this line to maintain total pulse energy[40,44]. The model shows mostly constant yield across the 2MJ contour, except with lower yields for low laser peak length (<4ns) and high laser peak power (>460 TW). For the same total laser energy, this model suggests that neutron yields for these three shots can be modestly improved with longer laser peak lengths and lower laser peak power. As stated earlier, this model has not observed an ignited shot, and therefore cannot predict ignition itself, but it can indicate the design space where we can expect at least as high yields as observed in past data. This region of high yield shots identified by the model below 2MJ would be an interested space to explore with other ML models [45] and more expensive conventional hydrodynamic simulations [46].

The yield prediction becomes unreliable beyond 2MJ because there is no data beyond that range in our dataset. We see that the yield generally plateaus in that regime, although the plots of N180128 and N220604 show an anomalously high predicted yield at a laser peak length of >4.75ns. The sharp nature of the contour is likely due to the decision tree-like structure of the GBDT regression model. In any case, this region lies in energy ranges far beyond what is included in the dataset, and so cannot be considered a valid prediction. Instead, this model should be used to predict yields for shot designs within the realm of observed laser energies.

Picket power and trough length

In Fig. 8b, the relationship of both the picket power and trough length are explored. These two parameters are linked together because the picket power greatly influences the speed of the 1st shock in the ablator and the trough length contributes to the timing of the 2nd shock and, together, determines where in the capsule they coalesce [47]. The surfaces in Fig. 8b does exhibit some linking between these parameters, although the overall scale of the difference in yield is significantly smaller than in Fig 8a. The model predicts slightly higher yields for N180128 and N220604 at higher trough length and lower laser picket power, while the model finds that N210808 already sits at an optimal value in this space. The region of increased yield in the upper left corner is an artifact of extrapolation. The dataset does not contain any values > 0.8ns for the trough length. One can also find evidence indicative of overfitting in this plot from the non-physical vertical and horizontal striations in the yield levels. These do not represent large differences in yield but do indicate that the model is not completely capturing the relevant physics. Overall, the model shows very little movement of the yield when these parameters are altered, this is likely due to the absence of experiments with relatively large changes in picket power and trough length.

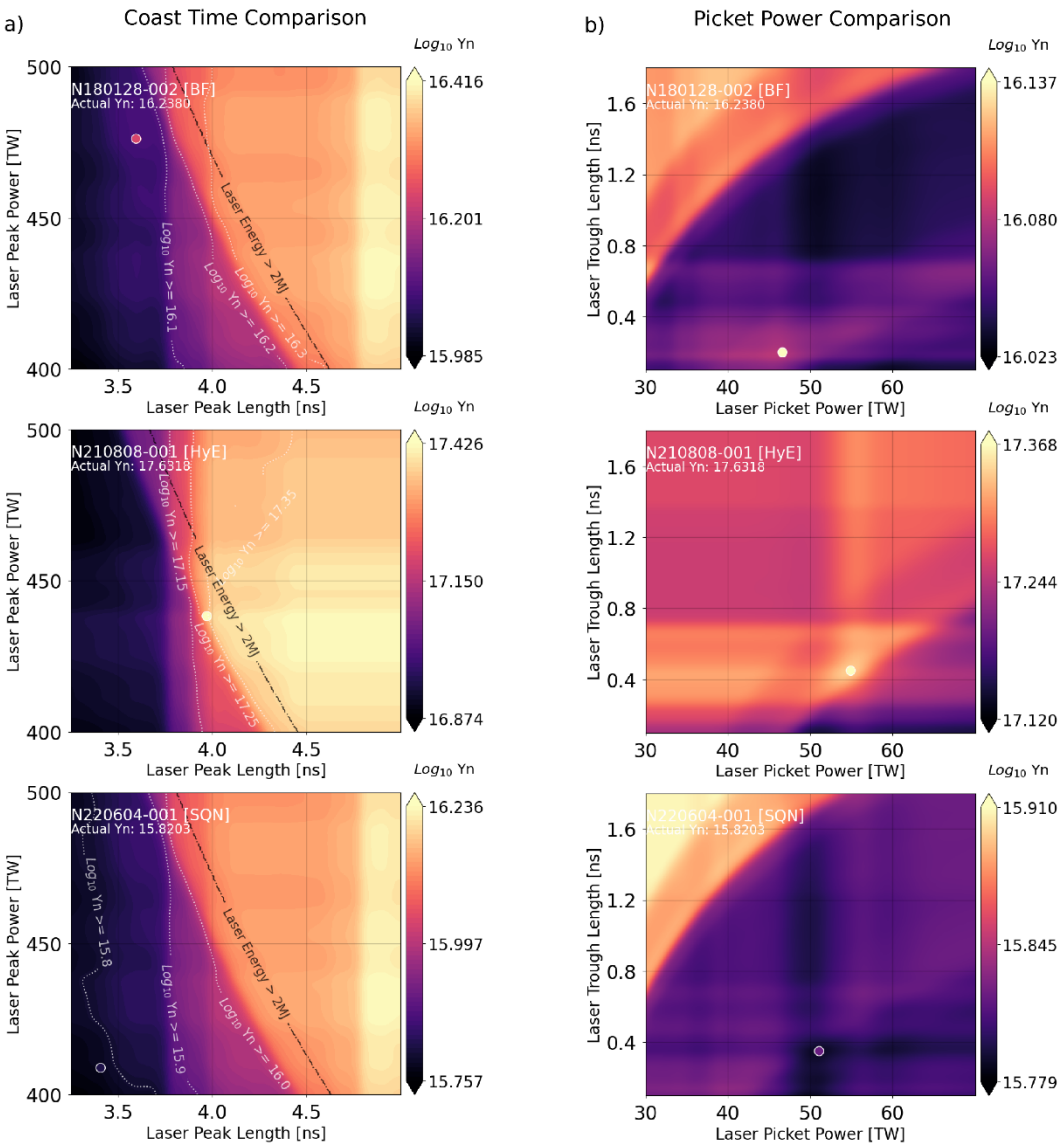

Figure 8: (a) The relationship of coast time (inverse of laser peak length) and laser peak power to the yield of N180128 [BigFoot],N210808 [Hybrid-E], and N220604 [SQ-n]. Note the difference in the bounds of the color scale in each plot. (b) The relationship of the picket power and the trough length of the yield to the same three experiments. Again, note the difference between color scales for each plot.

Laser picket cone fraction and $\Delta\lambda_{23}$

Parameters that are thought to affect the symmetry of the implosion are explored in Fig. 9a with the relationship of the laser picket cone fraction, $\Delta\lambda_{23}$, and yield. The laser picket cone fraction is deemed as the most important feature in the model, as shown in Fig. 6. By examining the range of values for the different campaigns, we see that the model is using both features to separate low and high yield shots in a way that does not reflect the underlying physics well. The overall difference in yield is smaller than on the laser energy plot in Fig. 8a but is not insignificant. Decision-tree based regression models can be thought of making predictions by carving up the input space using a decision-tree and assigning predictions to each location. As we see in Fig. 8, the GBDT architecture is able to learn more complex relationships than one-dimensional thresholds that you would find for a simple decision-tree regressor,

but in this case, the model disappointingly cannot identify the key physical relationships. We would expect a peak around yield at the $\Delta\lambda_{23}$ that generates a symmetric implosion. This exploration shows that these features, while ranking high on feature importance, appear to be missing the key physical relationships. Future work using this model to design shots should likely be cautious when optimizing these parameters. More data with a more diverse set of values for these parameters would help clear up the relationship, but future iterations of this model may also consider dropping these parameters from the learning process altogether. They may measure highly on feature importance, but they may also be responsible for the discrepancy between train error (train set MAPE: 18.8%) and test error (test set MAPE: 35.5%) discussed in section earlier. Alternatively, using a P2 (second Legendre mode used to measure how oblate or prolate the shape of the hot spot is) playbook derived from the Cone Fraction and/or the $\Delta\lambda_{23}$ could be used.

Fill tube size and K number

In Fig. 9b, we look at the relationship of the fill tube [48] size and the K number to the yield. These two features are not design choices but engineering limits. The fill tube is a 2, 5 or, 10 µm diameter tube required to fill the capsule with DT gas. It is known to also seed material that mixes into the hot spot while radiatively cooling it [49,50], thus reducing the resulting yield. The 2 µm diameter fill tube was implemented on very few shots prior to N210808, with most previous experiments having 5 µm or larger diameters. Nevertheless, the model still correctly identifies that yield degrades with larger fill tubes. There is no variation within the ~2, ~5 or, ~10 µm diameter tube ranges because only those three discrete values for fill tube sizes are used in practice. The "K number," on the other hand, has a smaller impact on the yield. The K number is a rms measure of the area and length of all defect grooves in the DT ice layer. The distribution of the K number among the different campaigns are close to uniform. Lower K number generally correlates with higher predicted yield, as we would expect, but there is a curious decrease in predicted yield at K number < 0.5. This is likely due to some amount of overfitting and a lack of much data in that range (there are not shots in our dataset with K number < 0.2). One would always expect a lower K-number to lead to higher yields all else constant, indicating that one additional pathway to improving the model would be to require during training that the yield prediction can never decrease with lower K-number. By requiring that known physical trends are respected by the model, we could counteract some amount of the overfitting we observe in this analysis.

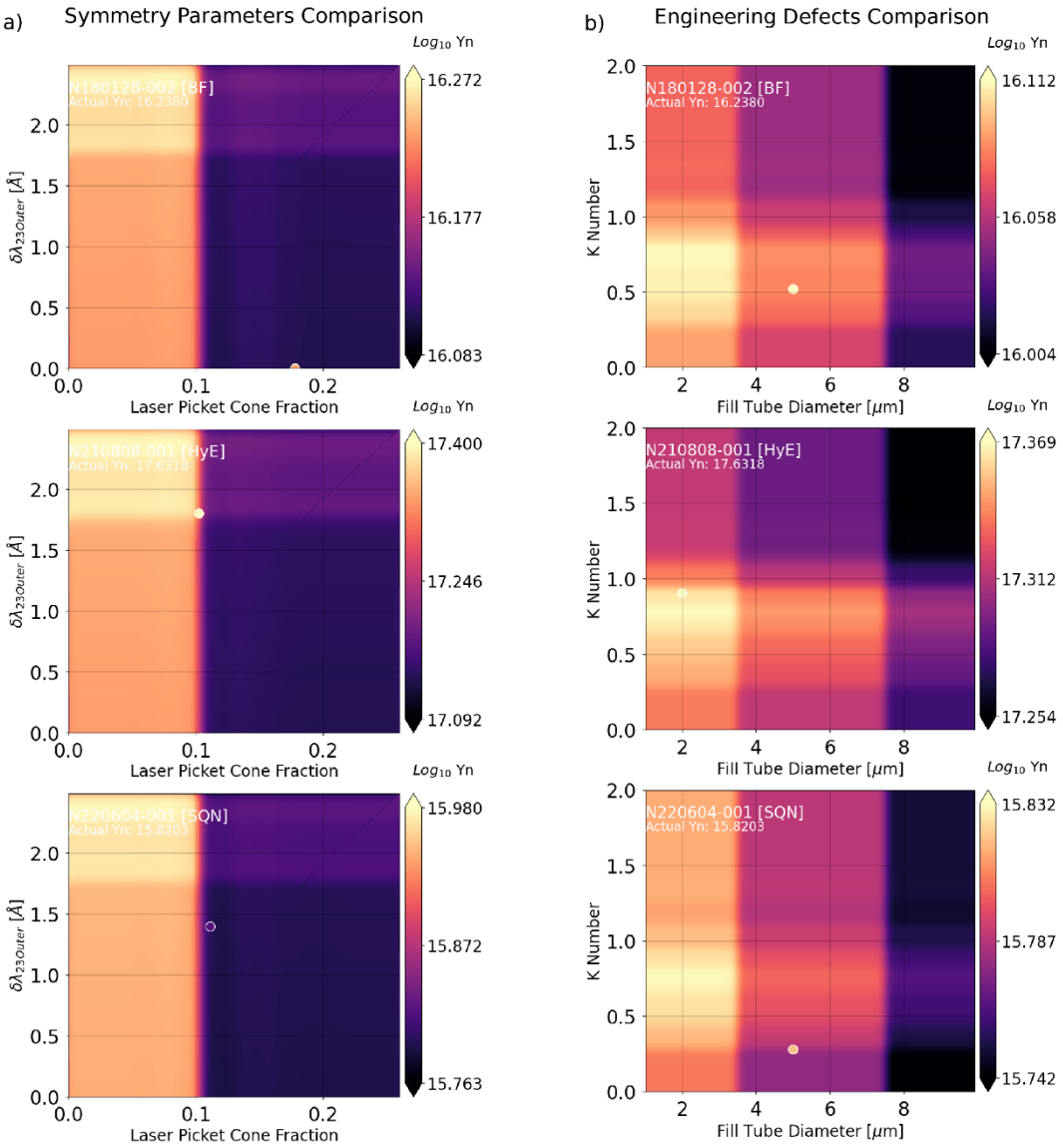

Figure 9: (a) The relationship of laser picket cone fraction and Δλ2-Δλ3 to the yield of N180128 [BigFoot],N210808 [Hybrid-E], and N220604 [SQ-n].. (b) The relationship of the fill tube diameter and the ice figure of merit K to the yield for the same three experiments. Again, the color bar is different in each plot.

4. Conclusion

In this paper, we evaluate the performance and physicality of neutron yield predictions and correlations produced by a machine learning model trained on only shot design and manufacturing data from NIF. For a randomly assigned test set, the model achieves 35.5% error on predicting the yield compared to the observed ~10-25% typical repeatability of identical shots at NIF. The overfitting exhibited in this model indicates opportunities for future work to build upon this model. We shed light on the inner workings of the model by utilizing the feature importance metrics of the GBDT architecture and by scaling the inputs of example shots. The model places a strong importance on features related to the ablation pressure, such as main pulse length, total laser energy, and LEH diameter, with secondary importance given to capsule quality. This is expected because the parameters for ablation pressure influences the compression at stagnation; optimizing the duration and extent of compression is

necessary for ignition. By varying the number of features in the model, we find that 25%-30% test error is achievable with this architecture on this task, but not consistently so; there are significant variations in performance as individual features are added, even when >20 features are already included in the model. This could be due to randomness in the architecture itself, the small number of test set examples, and/or the variations in the hyperparameter search. Future work may be able to achieve consistent performance improvements by exploring other hyperparameter search methods for a more robust alternative than utilized in this study.

Future improvements could also be achieved with an improved capsule quality metric. Capsule quality is recognized to be one of the key drivers of NIF shot performance, but without consistent quantitative measurements across the dataset, the capsule quality metric simply indicates before or after the discontinuous improvement in capsule quality for shot N210808. Future work could leverage the automated capsule quality measurement scheme under development and the ability of GBDTs to make predictions even when some data for certain parameters are missing (unlike neural networks). Refined capsule quality data would likely greatly improve ML-based yield predictions.

We took a closer look at how certain parameters affect the yield using experiments from three different campaigns as the starting point: N180128 (Big Foot campaign), N210808 (Hybrid E campaign), and N220604 (SQ-n campaign). For all three experiments, the model finds improvements in yield with higher laser energy, particular at intermediate peak length and laser power. Trends in other features indicate that the model is not always capturing physically realistic relationships, such with picket cone fraction. Future work could improve prediction accuracy (via reduced overfitting) by requiring that certain known physical relationships (such as yield cannot decrease as K number decreases) are enforced on the model and by gathering more experimental data in the regime of interest to the researchers, such as near-ignition or ignited shots.

Although this GBDT approach is limited in some ways, it complements other tools for designing and analyzing NIF shots by being as fast as 0-D yield estimates and capable of accounting for a variety of experimental settings. The methodology could find a place in between low fidelity analytic yield estimates and high-fidelity simulations. We note that the model will likely not achieve as good performance when extrapolating to unseen ignited regimes given the discontinuity in yield caused by alpha heating, but it could be used to quickly indicate that a particular shot design will at least be in the upper range of previously seen yields and close to the ignition threshold, even if this is just a lower bound. Additionally, users could leverage a standard “novelty detection" algorithm to determine whether a proposed experiment is similar enough to past data for this data-driven model to return a reliable prediction. Future work could also apply this approach to predicting other figures of merit, such as the Lawson product ($p\tau_E$) or downscatter ratio, which have different dependencies on the scale and energy than neutron yield.

Acknowledgements

The authors sincerely thank the NIF staff and researchers that helped make the DT shots possible. This work was performed under the auspices of the U.S. Department of Energy by Lawrence Livermore National Laboratory under Contract No. DE-AC52-07NA27344 and Release No. LLNL-JRNL-830845.

Bibliography

[1] G.H. Miller, E.I. Moses, and C.R. Wuest, Opt. Eng. **43**, 2841 (2004).
[2] A.B. Zylstra, O.A. Hurricane, D.A. Callahan, A.L. Kritcher, J.E. Ralph, H.F. Robey, J.S. Ross, C.V. Young, K.L. Baker, D.T. Casey, T. Döppner, L. Divol, M. Hohenberger, S. Le Pape, A. Pak, P.K. Patel, R. Tommasini, S.J. Ali, P.A. Amendt, L.J. Atherton, B. Bachmann, D. Bailey, L.R. Benedetti, L. Berzak Hopkins, R. Betti, S.D. Bhandarkar, J. Biener, R.M. Bionta, N.W. Birge, E.J. Bond, D.K. Bradley, T. Braun, T.M. Briggs, M.W. Bruhn, P.M. Celliers, B. Chang, T. Chapman, H. Chen, C. Choate, A.R. Christopherson, D.S. Clark, J.W. Crippen, E.L. Dewald, T.R. Dittrich, M.J. Edwards, W.A. Farmer, J.E. Field, D. Fittinghoff, J. Frenje, J. Gaffney, M. Gatu Johnson, S.H. Glenzer, G.P. Grim, S. Haan, K.D. Hahn, G.N. Hall, B.A. Hammel, J. Harte, E. Hartouni, J.E. Heebner, V.J. Hernandez, H. Herrmann, M.C. Herrmann, D.E. Hinkel, D.D. Ho, J.P. Holder, W.W. Hsing, H. Huang, K.D. Humbird, N. Izumi, L.C. Jarrott, J. Jeet, O. Jones, G.D. Kerbel, S.M. Kerr, S.F. Khan, J. Kilkenny, Y. Kim, H. Geppert Kleinrath, V. Geppert Kleinrath, C. Kong, J.M. Koning, J.J. Kroll, M.K.G. Kruse, B. Kustowski, O.L. Landen, S. Langer, D. Larson, N.C. Lemos, J.D. Lindl, T. Ma, M.J. MacDonald, B.J. MacGowan, A.J. Mackinnon, S.A. MacLaren, A.G. MacPhee, M.M. Marinak, D.A. Mariscal, E.V. Marley, L. Masse, K. Meaney, N.B. Meezan, P.A. Michel, M. Millot, J.L. Milovich, J.D. Moody, A.S. Moore, J.W. Morton, T. Murphy, K. Newman, J.-M.G. Di Nicola, A. Nikroo, R. Nora, M.V. Patel, L.J. Pelz, J.L. Peterson, Y. Ping, B.B. Pollock, M. Ratledge, N.G. Rice, H. Rinderknecht, M. Rosen, M.S. Rubery, J.D. Salmonson, J. Sater, S. Schiaffino, D.J. Schlossberg, M.B. Schneider, C.R. Schroeder, H.A. Scott, S.M. Sepke, K. Sequoia, M.W. Sherlock, S. Shin, V.A. Smalyuk, B.K. Spears, P.T. Springer, M. Stadermann, S. Stoupin, D.J. Strozzi, L.J. Suter, C.A. Thomas, R.P.J. Town, E.R. Tubman, P.L. Volegov, C.R. Weber, K. Widmann, C. Wild, C.H. Wilde, B.M. Van Wonterghem, D.T. Woods, B.N. Woodworth, M. Yamaguchi, S.T. Yang, and G.B. Zimmerman, Nature **601**, 542 (2022).
[3] J. Lindl, Phys. Plasmas **2**, 3933 (1995).
[4] D. Humphreys, A. Kupresanin, D. Boyer, J. Canik, E.C. Cyr, R. Granetz, J. Hittinger, E. Kolemen, E. Lawrence, and V. Pascucci, *Advancing Fusion with Machine Learning Research Needs Workshop* (USDOE Office of Science (SC) (United States), 2019).
[5] C. Rea, R.S. Granetz, K. Montes, R.A. Tinguely, N. Eidietis, J.M. Hanson, and B. Sammuli, Plasma Phys. Control. Fusion **60**, 084004 (2018).
[6](n.d.).
[7] M.S. Murillo, M. Marciante, and L.G. Stanton, Phys. Rev. Lett. **125**, 085503 (2020).
[8] M.A. Wood, M.A. Cusentino, B.D. Wirth, and A.P. Thompson, Phys. Rev. B **99**, 184305 (2019).
[9] E.A. Baltz, E. Trask, M. Binderbauer, M. Dikovsky, H. Gota, R. Mendoza, J.C. Platt, and P.F. Riley, Sci. Rep. **7**, 6425 (2017).
[10] V. Gopalaswamy, R. Betti, J.P. Knauer, N. Luciani, D. Patel, K.M. Woo, A. Bose, I.V. Igumenshchev, E.M. Campbell, K.S. Anderson, K.A. Bauer, M.J. Bonino, D. Cao, A.R. Christopherson, G.W. Collins, T.J.B. Collins, J.R. Davies, J.A. Delettrez, D.H. Edgell, R. Epstein, C.J. Forrest, D.H. Froula, V.Y. Glebov, V.N. Goncharov, D.R. Harding, S.X. Hu, D.W. Jacobs-Perkins, R.T. Janezic, J.H. Kelly, O.M. Mannion, A. Maximov, F.J. Marshall, D.T. Michel, S. Miller, S.F.B. Morse, J. Palastro, J. Peebles, P.B. Radha, S.P. Regan, S. Sampat, T.C. Sangster, A.B. Sefkow, W. Seka, R.C. Shah, W.T. Shmyada, A. Shvydky, C. Stoeckl, A.A. Solodov, W. Theobald, J.D. Zuegel, M.G. Johnson, R.D. Petrasso, C.K. Li, and J.A. Frenje, Nature **565**, 581 (2019).

[11] J.A. Gaffney, S.T. Brandon, K.D. Humbird, M.K.G. Kruse, R.C. Nora, J.L. Peterson, and B.K. Spears, Phys. Plasmas **26**, 082704 (2019).
[12] J.L. Peterson, K.D. Humbird, J.E. Field, S.T. Brandon, S.H. Langer, R.C. Nora, B.K. Spears, and P.T. Springer, Phys. Plasmas **24**, 032702 (2017).
[13] K.D. Humbird, J.L. Peterson, and R.G. McClarren, ArXiv181206055 Cs Stat (2018).
[14] J.B. Nakhleh, M.G. Fernández-Godino, M.J. Grosskopf, B.M. Wilson, J. Kline, and G. Srinivasan, IEEE Trans. Plasma Sci. 1 (2021).
[15] A. Hsu, B. Cheng, and P.A. Bradley, Phys. Plasmas **27**, 012703 (2020).
[16] J.H. Friedman, Ann. Stat. **29**, 1189 (2001).
[17] S.W. Haan, D.A. Callahan, M.J. Edwards, B.A. Hammel, D.D. Ho, O.S. Jones, J.D. Lindl, B.J. MacGOWAN, M.M. Marinak, D.H. Munro, S.M. Pollaine, J.D. Salmonson, B.K. Spears, and L.J. Suter, Fusion Sci. Technol. **55**, 227 (2009).
[18] R. Town, *Laser Indirect Drive Input to NNSA 2020 Report* (Lawrence Livermore National Lab. (LLNL), Livermore, CA (United States), 2020).
[19] R.P.J. Town, D.K. Bradley, A. Kritcher, O.S. Jones, J.R. Rygg, R. Tommasini, M. Barrios, L.R. Benedetti, L.F. Berzak Hopkins, P.M. Celliers, T. Döppner, E.L. Dewald, D.C. Eder, J.E. Field, S.M. Glenn, N. Izumi, S.W. Haan, S.F. Khan, J.L. Kline, G.A. Kyrala, T. Ma, J.L. Milovich, J.D. Moody, S.R. Nagel, A. Pak, J.L. Peterson, H.F. Robey, J.S. Ross, R.H.H. Scott, B.K. Spears, M.J. Edwards, J.D. Kilkenny, and O.L. Landen, Phys. Plasmas **21**, 056313 (2014).
[20] H. Abu-Shawareb, R. Acree, P. Adams, J. Adams, B. Addis, R. Aden, P. Adrian, B.B. Afeyan, M. Aggleton, L. Aghaian, A. Aguirre, D. Aikens, J. Akre, F. Albert, M. Albrecht, B.J. Albright, J. Albritton, J. Alcala, C. Alday, D.A. Alessi, N. Alexander, J. Alfonso, N. Alfonso, E. Alger, S.J. Ali, Z.A. Ali, W.E. Alley, P. Amala, P.A. Amendt, P. Amick, S. Ammula, C. Amorin, D.J. Ampleford, R.W. Anderson, T. Anklam, N. Antipa, B. Appelbe, C. Aracne-Ruddle, E. Araya, M. Arend, P. Arnold, T. Arnold, J. Asay, L.J. Atherton, D. Atkinson, R. Atkinson, J.M. Auerbach, B. Austin, L. Auyang, A.S. Awwal, J. Ayers, S. Ayers, T. Ayers, S. Azevedo, B. Bachmann, C.A. Back, J. Bae, D.S. Bailey, J. Bailey, T. Baisden, K.L. Baker, H. Baldis, D. Barber, M. Barberis, D. Barker, A. Barnes, C.W. Barnes, M.A. Barrios, C. Barty, I. Bass, S.H. Batha, S.H. Baxamusa, G. Bazan, J.K. Beagle, R. Beale, B.R. Beck, J.B. Beck, M. Bedzyk, R.G. Beeler, R.G. Beeler, W. Behrendt, L. Belk, P. Bell, M. Belyaev, J.F. Benage, G. Bennett, L.R. Benedetti, L.X. Benedict, R. Berger, T. Bernat, L.A. Bernstein, B. Berry, L. Bertolini, G. Besenbruch, J. Betcher, R. Bettenhausen, R. Betti, B. Bezzerides, S.D. Bhandarkar, R. Bickel, J. Biener, T. Biesiada, K. Bigelow, J. Bigelow-Granillo, V. Bigman, R.M. Bionta, N.W. Birge, M. Bitter, A.C. Black, R. Bleile, D.L. Bleuel, E. Bliss, E. Bliss, B. Blue, T. Boehly, K. Boehm, C.D. Boley, R. Bonanno, E.J. Bond, T. Bond, M.J. Bonino, M. Borden, J.-L. Bourgade, J. Bousquet, J. Bowers, M. Bowers, R. Boyd, A. Bozek, D.K. Bradley, K.S. Bradley, P.A. Bradley, L. Bradley, L. Brannon, P.S. Brantley, D. Braun, T. Braun, K. Brienza-Larsen, T.M. Briggs, J. Britten, E.D. Brooks, D. Browning, M.W. Bruhn, T.A. Brunner, H. Bruns, G. Brunton, B. Bryant, T. Buczek, J. Bude, L. Buitano, S. Burkhart, J. Burmark, A. Burnham, R. Burr, L.E. Busby, B. Butlin, R. Cabeltis, M. Cable, W.H. Cabot, B. Cagadas, J. Caggiano, R. Cahayag, S.E. Caldwell, S. Calkins, D.A. Callahan, J. Calleja-Aguirre, L. Camara, D. Camp, E.M. Campbell, J.H. Campbell, B. Carey, R. Carey, K. Carlisle, L. Carlson, L. Carman, J. Carmichael, A. Carpenter, C. Carr, J.A. Carrera, D. Casavant, A. Casey, D.T. Casey, A. Castillo, E. Castillo, J.I. Castor, C. Castro, W. Caughey, R. Cavitt, J. Celeste, P.M. Celliers, C. Cerjan, G. Chandler, B. Chang, C. Chang, J. Chang, L. Chang, R. Chapman, T. Chapman, L. Chase, H. Chen, H. Chen, K. Chen, L.-Y. Chen, B. Cheng, J. Chittenden, C. Choate, J. Chou, R.E. Chrien, M. Chrisp, K. Christensen, M.

Christensen, A.R. Christopherson, M. Chung, J.A. Church, A. Clark, D.S. Clark, K. Clark, R. Clark, L. Claus, B. Cline, J.A. Cline, J.A. Cobble, K. Cochrane, B. Cohen, S. Cohen, M.R. Collette, G. Collins, L.A. Collins, T.J.B. Collins, A. Conder, B. Conrad, M. Conyers, A.W. Cook, D. Cook, R. Cook, J.C. Cooley, G. Cooper, T. Cope, S.R. Copeland, F. Coppari, J. Cortez, J. Cox, D.H. Crandall, J. Crane, R.S. Craxton, M. Cray, A. Crilly, J.W. Crippen, D. Cross, M. Cuneo, G. Cuotts, C.E. Czajka, D. Czechowicz, T. Daly, P. Danforth, R. Darbee, B. Darlington, P. Datte, L. Dauffy, G. Davalos, S. Davidovits, P. Davis, J. Davis, S. Dawson, R.D. Day, T.H. Day, M. Dayton, C. Deck, C. Decker, C. Deeney, K.A. DeFriend, G. Deis, N.D. Delamater, J.A. Delettrez, R. Demaret, S. Demos, S.M. Dempsey, R. Desjardin, T. Desjardins, M.P. Desjarlais, E.L. Dewald, J. DeYoreo, S. Diaz, G. Dimonte, T.R. Dittrich, L. Divol, S.N. Dixit, J. Dixon, E.S. Dodd, D. Dolan, A. Donovan, M. Donovan, T. Döppner, C. Dorrer, N. Dorsano, M.R. Douglas, D. Dow, J. Downie, E. Downing, M. Dozieres, V. Draggoo, D. Drake, R.P. Drake, T. Drake, G. Dreifuerst, D.F. DuBois, P.F. DuBois, G. Dunham, R. Dylla-Spears, A.K.L. Dymoke-Bradshaw, B. Dzenitis, C. Ebbers, M. Eckart, S. Eddinger, D. Eder, D. Edgell, M.J. Edwards, P. Efthimion, J.H. Eggert, B. Ehrlich, P. Ehrmann, S. Elhadj, C. Ellerbee, N.S. Elliott, C.L. Ellison, F. Elsner, M. Emerich, K. Engelhorn, T. England, E. English, P. Epperson, R. Epstein, G. Erbert, M.A. Erickson, D.J. Erskine, A. Erlandson, R.J. Espinosa, C. Estes, K.G. Estabrook, S. Evans, A. Fabyan, J. Fair, R. Fallejo, N. Farmer, W.A. Farmer, M. Farrell, V.E. Fatherley, M. Fedorov, E. Feigenbaum, M. Feit, W. Ferguson, J.C. Fernandez, A. Fernandez-Panella, S. Fess, J.E. Field, C.V. Filip, J.R. Fincke, T. Finn, S.M. Finnegan, R.G. Finucane, M. Fischer, A. Fisher, J. Fisher, B. Fishler, D. Fittinghoff, P. Fitzsimmons, M. Flegel, K.A. Flippo, J. Florio, J. Folta, P. Folta, L.R. Foreman, C. Forrest, A. Forsman, J. Fooks, M. Foord, R. Fortner, K. Fournier, D.E. Fratanduono, N. Frazier, T. Frazier, C. Frederick, M.S. Freeman, J. Frenje, D. Frey, G. Frieders, S. Friedrich, D.H. Froula, J. Fry, T. Fuller, J. Gaffney, S. Gales, B. Le Galloudec, K.K. Le Galloudec, A. Gambhir, L. Gao, W.J. Garbett, A. Garcia, C. Gates, E. Gaut, P. Gauthier, Z. Gavin, J. Gaylord, M. Geissel, F. Génin, J. Georgeson, H. Geppert-Kleinrath, V. Geppert-Kleinrath, N. Gharibyan, J. Gibson, C. Gibson, E. Giraldez, V. Glebov, S.G. Glendinning, S. Glenn, S.H. Glenzer, S. Goade, P.L. Gobby, S.R. Goldman, B. Golick, M. Gomez, V. Goncharov, D. Goodin, P. Grabowski, E. Grafil, P. Graham, J. Grandy, E. Grasz, F. Graziani, G. Greenman, J.A. Greenough, A. Greenwood, G. Gregori, T. Green, J.R. Griego, G.P. Grim, J. Grondalski, S. Gross, J. Guckian, N. Guler, B. Gunney, G. Guss, S. Haan, J. Hackbarth, L. Hackel, R. Hackel, C. Haefner, C. Hagmann, K.D. Hahn, S. Hahn, B.J. Haid, B.M. Haines, B.M. Hall, C. Hall, G.N. Hall, M. Hamamoto, S. Hamel, C.E. Hamilton, B.A. Hammel, J.H. Hammer, G. Hampton, A. Hamza, A. Handler, S. Hansen, D. Hanson, R. Haque, D. Harding, E. Harding, J.D. Hares, D.B. Harris, J.A. Harte, E.P. Hartouni, R. Hatarik, S. Hatchett, A.A. Hauer, M. Havre, R. Hawley, J. Hayes, J. Hayes, S. Hayes, A. Hayes-Sterbenz, C.A. Haynam, D.A. Haynes, D. Headley, A. Heal, J.E. Heebner, S. Heerey, G.M. Heestand, R. Heeter, N. Hein, C. Heinbockel, C. Hendricks, M. Henesian, J. Heninger, J. Henrikson, E.A. Henry, E.B. Herbold, M.R. Hermann, G. Hermes, J.E. Hernandez, V.J. Hernandez, M.C. Herrmann, H.W. Herrmann, O.D. Herrera, D. Hewett, R. Hibbard, D.G. Hicks, D. Hill, K. Hill, T. Hilsabeck, D.E. Hinkel, D.D. Ho, V.K. Ho, J.K. Hoffer, N.M. Hoffman, M. Hohenberger, M. Hohensee, W. Hoke, D. Holdener, F. Holdener, J.P. Holder, B. Holko, D. Holunga, J.F. Holzrichter, J. Honig, D. Hoover, D. Hopkins, L. Berzak Hopkins, M. Hoppe, M.L. Hoppe, J. Horner, R. Hornung, C.J. Horsfield, J. Horvath, D. Hotaling, R. House, L. Howell, W.W. Hsing, S.X. Hu, H. Huang, J. Huckins, H. Hui, K.D. Humbird, J. Hund, J. Hunt, O.A. Hurricane, M. Hutton, K.H.-K. Huynh, L. Inandan, C. Iglesias, I.V. Igumenshchev, N. Izumi, M. Jackson, J. Jackson, S.D. Jacobs, G. James, K.

Jancaitis, J. Jarboe, L.C. Jarrott, D. Jasion, J. Jaquez, J. Jeet, A.E. Jenei, J. Jensen, J. Jimenez, R. Jimenez, D. Jobe, Z. Johal, H.M. Johns, D. Johnson, M.A. Johnson, M. Gatu Johnson, R.J. Johnson, S. Johnson, S.A. Johnson, T. Johnson, K. Jones, O. Jones, M. Jones, R. Jorge, H.J. Jorgenson, M. Julian, B.I. Jun, R. Jungquist, J. Kaae, N. Kabadi, D. Kaczala, D. Kalantar, K. Kangas, V.V. Karasiev, M. Karasik, V. Karpenko, A. Kasarky, K. Kasper, R. Kauffman, M.I. Kaufman, C. Keane, L. Keaty, L. Kegelmeyer, P.A. Keiter, P.A. Kellett, J. Kellogg, J.H. Kelly, S. Kemic, A.J. Kemp, G.E. Kemp, G.D. Kerbel, D. Kershaw, S.M. Kerr, T.J. Kessler, M.H. Key, S.F. Khan, H. Khater, C. Kiikka, J. Kilkenny, Y. Kim, Y.-J. Kim, J. Kimko, M. Kimmel, J.M. Kindel, J. King, R.K. Kirkwood, L. Klaus, D. Klem, J.L. Kline, J. Klingmann, G. Kluth, P. Knapp, J. Knauer, J. Knipping, M. Knudson, D. Kobs, J. Koch, T. Kohut, C. Kong, J.M. Koning, P. Koning, S. Konior, H. Kornblum, L.B. Kot, B. Kozioziemski, M. Kozlowski, P.M. Kozlowski, J. Krammen, N.S. Krasheninnikova, B. Kraus, W. Krauser, J.D. Kress, A.L. Kritcher, E. Krieger, J.J. Kroll, W.L. Kruer, M.K.G. Kruse, S. Kucheyev, M. Kumbera, S. Kumpan, J. Kunimune, B. Kustowski, T.J.T. Kwan, G.A. Kyrala, S. Laffite, M. Lafon, K. LaFortune, B. Lahmann, B. Lairson, O.L. Landen, J. Langenbrunner, L. Lagin, T. Land, M. Lane, D. Laney, A.B. Langdon, S.H. Langer, A. Langro, N.E. Lanier, T.E. Lanier, D. Larson, B.F. Lasinski, D. Lassle, D. LaTray, G. Lau, N. Lau, C. Laumann, A. Laurence, T.A. Laurence, J. Lawson, H.P. Le, R.R. Leach, L. Leal, A. Leatherland, K. LeChien, B. Lechleiter, A. Lee, M. Lee, T. Lee, R.J. Leeper, E. Lefebvre, J.-P. Leidinger, B. LeMire, R.W. Lemke, N.C. Lemos, S. Le Pape, R. Lerche, S. Lerner, S. Letts, K. Levedahl, T. Lewis, C.K. Li, H. Li, J. Li, W. Liao, Z.M. Liao, D. Liedahl, J. Liebman, G. Lindford, E.L. Lindman, J.D. Lindl, H. Loey, R.A. London, F. Long, E.N. Loomis, F.E. Lopez, H. Lopez, E. Losbanos, S. Loucks, R. Lowe-Webb, E. Lundgren, A.P. Ludwigsen, R. Luo, J. Lusk, R. Lyons, T. Ma, Y. Macallop, M.J. MacDonald, B.J. MacGowan, J.M. Mack, A.J. Mackinnon, S.A. MacLaren, A.G. MacPhee, G.R. Magelssen, J. Magoon, R.M. Malone, T. Malsbury, R. Managan, R. Mancini, K. Manes, D. Maney, D. Manha, O.M. Mannion, A.M. Manuel, E. Mapoles, G. Mara, T. Marcotte, E. Marin, M.M. Marinak, C. Mariscal, D.A. Mariscal, E.F. Mariscal, E.V. Marley, J.A. Marozas, R. Marquez, C.D. Marshall, F.J. Marshall, M. Marshall, S. Marshall, J. Marticorena, D. Martinez, I. Maslennikov, D. Mason, R.J. Mason, L. Masse, W. Massey, P.-E. Masson-Laborde, N.D. Masters, D. Mathisen, E. Mathison, J. Matone, M.J. Matthews, C. Mattoon, T.R. Mattsson, K. Matzen, C.W. Mauche, M. Mauldin, T. McAbee, M. McBurney, T. Mccarville, R.L. McCrory, A.M. McEvoy, C. McGuffey, M. Mcinnis, P. McKenty, M.S. McKinley, J.B. McLeod, A. McPherson, B. Mcquillan, M. Meamber, K.D. Meaney, N.B. Meezan, R. Meissner, T.A. Mehlhorn, N.C. Mehta, J. Menapace, F.E. Merrill, B.T. Merritt, E.C. Merritt, D.D. Meyerhofer, S. Mezyk, R.J. Mich, P.A. Michel, D. Milam, C. Miller, D. Miller, D.S. Miller, E. Miller, E.K. Miller, J. Miller, M. Miller, P.E. Miller, T. Miller, W. Miller, V. Miller-Kamm, M. Millot, J.L. Milovich, P. Minner, J.-L. Miquel, S. Mitchell, K. Molvig, R.C. Montesanti, D.S. Montgomery, M. Monticelli, A. Montoya, J.D. Moody, A.S. Moore, E. Moore, M. Moran, J.C. Moreno, K. Moreno, B.E. Morgan, T. Morrow, J.W. Morton, E. Moses, K. Moy, R. Muir, M.S. Murillo, J.E. Murray, J.R. Murray, D.H. Munro, T.J. Murphy, F.M. Munteanu, J. Nafziger, T. Nagayama, S.R. Nagel, R. Nast, R.A. Negres, A. Nelson, D. Nelson, J. Nelson, S. Nelson, S. Nemethy, P. Neumayer, K. Newman, M. Newton, H. Nguyen, J.-M.G. Di Nicola, P. Di Nicola, C. Niemann, A. Nikroo, P.M. Nilson, A. Nobile, V. Noorai, R. Nora, M. Norton, M. Nostrand, V. Note, S. Novell, P.F. Nowak, A. Nunez, R.A. Nyholm, M. O'Brien, A. Oceguera, J.A. Oertel, J. Okui, B. Olejniczak, J. Oliveira, P. Olsen, B. Olson, K. Olson, R.E. Olson, Y.P. Opachich, N. Orsi, C.D. Orth, M. Owen, S. Padalino, E. Padilla, R. Paguio, S. Paguio, J. Paisner, S. Pajoom, A. Pak, S.

Palaniyappan, K. Palma, T. Pannell, F. Papp, D. Paras, T. Parham, H.-S. Park, A. Pasternak, S. Patankar, M.V. Patel, P.K. Patel, R. Patterson, S. Patterson, B. Paul, M. Paul, E. Pauli, O.T. Pearce, J. Pearcy, B. Pedrotti, A. Peer, L.J. Pelz, B. Penetrante, J. Penner, A. Perez, L.J. Perkins, E. Pernice, T.S. Perry, S. Person, D. Petersen, T. Petersen, D.L. Peterson, E.B. Peterson, J.E. Peterson, J.L. Peterson, K. Peterson, R.R. Peterson, R.D. Petrasso, F. Philippe, T.J. Phipps, E. Piceno, Y. Ping, L. Pickworth, J. Pino, R. Plummer, G.D. Pollack, S.M. Pollaine, B.B. Pollock, D. Ponce, J. Ponce, J. Pontelandolfo, J.L. Porter, J. Post, O. Poujade, C. Powell, H. Powell, G. Power, M. Pozulp, M. Prantil, M. Prasad, S. Pratuch, S. Price, K. Primdahl, S. Prisbrey, R. Procassini, A. Pruyne, B. Pudliner, S.R. Qiu, K. Quan, M. Quinn, J. Quintenz, P.B. Radha, F. Rainer, J.E. Ralph, K.S. Raman, R. Raman, P. Rambo, S. Rana, A. Randewich, D. Rardin, M. Ratledge, N. Ravelo, F. Ravizza, M. Rayce, A. Raymond, B. Raymond, B. Reed, C. Reed, S. Regan, B. Reichelt, V. Reis, S. Reisdorf, V. Rekow, B.A. Remington, A. Rendon, W. Requieron, M. Rever, H. Reynolds, J. Reynolds, J. Rhodes, M. Rhodes, M.C. Richardson, B. Rice, N.G. Rice, R. Rieben, A. Rigatti, S. Riggs, H.G. Rinderknecht, K. Ring, B. Riordan, R. Riquier, C. Rivers, D. Roberts, V. Roberts, G. Robertson, H.F. Robey, J. Robles, P. Rocha, G. Rochau, J. Rodriguez, S. Rodriguez, M. Rosen, M. Rosenberg, G. Ross, J.S. Ross, P. Ross, J. Rouse, D. Rovang, A.M. Rubenchik, M.S. Rubery, C.L. Ruiz, M. Rushford, B. Russ, J.R. Rygg, B.S. Ryujin, R.A. Sacks, R.F. Sacks, K. Saito, T. Salmon, J.D. Salmonson, J. Sanchez, S. Samuelson, M. Sanchez, C. Sangster, A. Saroyan, J. Sater, A. Satsangi, S. Sauers, R. Saunders, J.P. Sauppe, R. Sawicki, D. Sayre, M. Scanlan, K. Schaffers, G.T. Schappert, S. Schiaffino, D.J. Schlossberg, D.W. Schmidt, M.J. Schmitt, D.H.G. Schneider, M.B. Schneider, R. Schneider, M. Schoff, M. Schollmeier, M. Schölmerich, C.R. Schroeder, S.E. Schrauth, H.A. Scott, I. Scott, J.M. Scott, R.H.H. Scott, C.R. Scullard, T. Sedillo, F.H. Seguin, W. Seka, J. Senecal, S.M. Sepke, L. Seppala, K. Sequoia, J. Severyn, J.M. Sevier, N. Sewell, S. Seznec, R.C. Shah, J. Shamlian, D. Shaughnessy, M. Shaw, R. Shaw, C. Shearer, R. Shelton, N. Shen, M.W. Sherlock, A.I. Shestakov, E.L. Shi, S.J. Shin, N. Shingleton, W. Shmayda, M. Shor, M. Shoup, C. Shuldberg, L. Siegel, F.J. Silva, A.N. Simakov, B.T. Sims, D. Sinars, P. Singh, H. Sio, K. Skulina, S. Skupsky, S. Slutz, M. Sluyter, V.A. Smalyuk, D. Smauley, R.M. Smeltser, C. Smith, I. Smith, J. Smith, L. Smith, R. Smith, R. Sohn, S. Sommer, C. Sorce, M. Sorem, J.M. Soures, M.L. Spaeth, B.K. Spears, S. Speas, D. Speck, R. Speck, J. Spears, T. Spinka, P.T. Springer, M. Stadermann, B. Stahl, J. Stahoviak, L.G. Stanton, R. Steele, W. Steele, D. Steinman, R. Stemke, R. Stephens, S. Sterbenz, P. Sterne, D. Stevens, J. Stevers, C.B. Still, C. Stoeckl, W. Stoeffl, J.S. Stolken, C. Stolz, E. Storm, G. Stone, S. Stoupin, E. Stout, I. Stowers, R. Strauser, H. Streckart, J. Streit, D.J. Strozzi, T. Suratwala, G. Sutcliffe, L.J. Suter, S.B. Sutton, V. Svidzinski, G. Swadling, W. Sweet, A. Szoke, M. Tabak, M. Takagi, A. Tambazidis, V. Tang, M. Taranowski, L.A. Taylor, S. Telford, W. Theobald, M. Thi, A. Thomas, C.A. Thomas, I. Thomas, R. Thomas, I.J. Thompson, A. Thongstisubskul, C.B. Thorsness, G. Tietbohl, R.E. Tipton, M. Tobin, N. Tomlin, R. Tommasini, A.J. Toreja, J. Torres, R.P.J. Town, S. Townsend, J. Trenholme, A. Trivelpiece, C. Trosseille, H. Truax, D. Trummer, S. Trummer, T. Truong, D. Tubbs, E.R. Tubman, T. Tunnell, D. Turnbull, R.E. Turner, M. Ulitsky, R. Upadhye, J.L. Vaher, P. VanArsdall, D. VanBlarcom, M. Vandenboomgaerde, R. VanQuinlan, B.M. Van Wonterghem, W.S. Varnum, A.L. Velikovich, A. Vella, C.P. Verdon, B. Vermillion, S. Vernon, R. Vesey, J. Vickers, R.M. Vignes, M. Visosky, J. Vocke, P.L. Volegov, S. Vonhof, R. Von Rotz, H.X. Vu, M. Vu, D. Wall, J. Wall, R. Wallace, B. Wallin, D. Walmer, C.A. Walsh, C.F. Walters, C. Waltz, A. Wan, A. Wang, Y. Wang, J.S. Wark, B.E. Warner, J. Watson, R.G. Watt, P. Watts, J. Weaver, R.P. Weaver, S. Weaver, C.R. Weber, P. Weber, S.V. Weber, P. Wegner, B. Welday, L. Welser-Sherrill, K.

Weiss, K. Widmann, G.F. Wheeler, W. Whistler, R.K. White, H.D. Whitley, P. Whitman, M.E. Wickett, C. Widmayer, J. Wiedwald, R. Wilcox, S. Wilcox, C. Wild, B.H. Wilde, C.H. Wilde, K. Wilhelmsen, M.D. Wilke, H. Wilkens, P. Wilkins, S.C. Wilks, E.A. Williams, G.J. Williams, W. Williams, W.H. Williams, D.C. Wilson, B. Wilson, E. Wilson, R. Wilson, S. Winters, J. Wisoff, M. Wittman, J. Wolfe, A. Wong, K.W. Wong, L. Wong, N. Wong, R. Wood, D. Woodhouse, J. Woodruff, D.T. Woods, S. Woods, B.N. Woodworth, E. Wooten, A. Wootton, K. Work, J.B. Workman, J. Wright, M. Wu, C. Wuest, F.J. Wysocki, H. Xu, M. Yamaguchi, B. Yang, S.T. Yang, J. Yatabe, C.B. Yeamans, B.C. Yee, S.A. Yi, L. Yin, B. Young, C.S. Young, C.V. Young, P. Young, K. Youngblood, R. Zacharias, G. Zagaris, N. Zaitseva, F. Zaka, F. Ze, B. Zeiger, M. Zika, G.B. Zimmerman, T. Zobrist, J.D. Zuegel, A.B. Zylstra, and Indirect Drive ICF Collaboration, Phys. Rev. Lett. **129**, 075001 (2022).

[21] A.L. Kritcher, A.B. Zylstra, D.A. Callahan, O.A. Hurricane, C.R. Weber, D.S. Clark, C.V. Young, J.E. Ralph, D.T. Casey, A. Pak, O.L. Landen, B. Bachmann, K.L. Baker, L. Berzak Hopkins, S.D. Bhandarkar, J. Biener, R.M. Bionta, N.W. Birge, T. Braun, T.M. Briggs, P.M. Celliers, H. Chen, C. Choate, L. Divol, T. Döppner, D. Fittinghoff, M.J. Edwards, M. Gatu Johnson, N. Gharibyan, S. Haan, K.D. Hahn, E. Hartouni, D.E. Hinkel, D.D. Ho, M. Hohenberger, J.P. Holder, H. Huang, N. Izumi, J. Jeet, O. Jones, S.M. Kerr, S.F. Khan, H. Geppert Kleinrath, V. Geppert Kleinrath, C. Kong, K.M. Lamb, S. Le Pape, N.C. Lemos, J.D. Lindl, B.J. MacGowan, A.J. Mackinnon, A.G. MacPhee, E.V. Marley, K. Meaney, M. Millot, A.S. Moore, K. Newman, J.-M.G. Di Nicola, A. Nikroo, R. Nora, P.K. Patel, N.G. Rice, M.S. Rubery, J. Sater, D.J. Schlossberg, S.M. Sepke, K. Sequoia, S.J. Shin, M. Stadermann, S. Stoupin, D.J. Strozzi, C.A. Thomas, R. Tommasini, C. Trosseille, E.R. Tubman, P.L. Volegov, C. Wild, D.T. Woods, and S.T. Yang, Phys. Rev. E **106**, 025201 (2022).

[22] A.B. Zylstra, A.L. Kritcher, O.A. Hurricane, D.A. Callahan, J.E. Ralph, D.T. Casey, A. Pak, O.L. Landen, B. Bachmann, K.L. Baker, L. Berzak Hopkins, S.D. Bhandarkar, J. Biener, R.M. Bionta, N.W. Birge, T. Braun, T.M. Briggs, P.M. Celliers, H. Chen, C. Choate, D.S. Clark, L. Divol, T. Döppner, D. Fittinghoff, M.J. Edwards, M. Gatu Johnson, N. Gharibyan, S. Haan, K.D. Hahn, E. Hartouni, D.E. Hinkel, D.D. Ho, M. Hohenberger, J.P. Holder, H. Huang, N. Izumi, J. Jeet, O. Jones, S.M. Kerr, S.F. Khan, H. Geppert Kleinrath, V. Geppert Kleinrath, C. Kong, K.M. Lamb, S. Le Pape, N.C. Lemos, J.D. Lindl, B.J. MacGowan, A.J. Mackinnon, A.G. MacPhee, E.V. Marley, K. Meaney, M. Millot, A.S. Moore, K. Newman, J.-M.G. Di Nicola, A. Nikroo, R. Nora, P.K. Patel, N.G. Rice, M.S. Rubery, J. Sater, D.J. Schlossberg, S.M. Sepke, K. Sequoia, S.J. Shin, M. Stadermann, S. Stoupin, D.J. Strozzi, C.A. Thomas, R. Tommasini, C. Trosseille, E.R. Tubman, P.L. Volegov, C.R. Weber, C. Wild, D.T. Woods, S.T. Yang, and C.V. Young, Phys. Rev. E **106**, 025202 (2022).

[23] A.J. MacKinnon, N.B. Meezan, J.S. Ross, S. Le Pape, L. Berzak Hopkins, L. Divol, D. Ho, J. Milovich, A. Pak, J. Ralph, T. Döppner, P.K. Patel, C. Thomas, R. Tommasini, S. Haan, A.G. MacPhee, J. McNaney, J. Caggiano, R. Hatarik, R. Bionta, T. Ma, B. Spears, J.R. Rygg, L.R. Benedetti, R.P.J. Town, D.K. Bradley, E.L. Dewald, D. Fittinghoff, O.S. Jones, H.R. Robey, J.D. Moody, S. Khan, D.A. Callahan, A. Hamza, J. Biener, P.M. Celliers, D.G. Braun, D.J. Erskine, S.T. Prisbrey, R.J. Wallace, B. Kozioziemski, R. Dylla-Spears, J. Sater, G. Collins, E. Storm, W. Hsing, O. Landen, J.L. Atherton, J.D. Lindl, M.J. Edwards, J.A. Frenje, M. Gatu-Johnson, C.K. Li, R. Petrasso, H. Rinderknecht, M. Rosenberg, F.H. Séguin, A. Zylstra, J.P. Knauer, G. Grim, N. Guler, F. Merrill, R. Olson, G.A. Kyrala, J.D. Kilkenny, A. Nikroo, K. Moreno, D.E. Hoover, C. Wild, and E. Werner, Phys. Plasmas **21**, 056318 (2014).

[24] L. Divol, A. Pak, L.F. Berzak Hopkins, S.L. Pape, N.B. Meezan, E.L. Dewald, D.D.-M. Ho, S.F. Khan, A.J. Mackinnon, J.S. Ross, D.P. Turnbull, C. Weber, P.M. Celliers, M. Millot, L.R. Benedetti, J.E. Field, N. Izumi, G.A. Kyrala, T. Ma, S.R. Nagel, J.R. Rygg, D. Edgell, A.G. Macphee, C. Goyon, M. Hohenberger, B.J. MacGowan, P. Michel, D. Strozzi, W.S. Cassata, D. Casey, D.N. Fittinghoff, N. Gharibyan, R. Hatarik, D. Sayre, P. Volegov, C. Yeamans, B. Bachmann, T. Döppner, J. Biener, J. Crippen, C. Choate, H. Huang, C. Kong, A. Nikroo, N.G. Rice, M. Stadermann, S.D. Bhandarkar, S. Haan, B. Kozioziemski, W.W. Hsing, O.L. Landen, J.D. Moody, R.P.J. Town, D.A. Callahan, O.A. Hurricane, and M.J. Edwards, Phys. Plasmas **24**, 056309 (2017).
[25] J.S. Ross, D. Ho, J. Milovich, T. Döppner, J. McNaney, A.G. MacPhee, A. Hamza, J. Biener, H.F. Robey, E.L. Dewald, R. Tommasini, L. Divol, S. Le Pape, L.B. Hopkins, P.M. Celliers, O. Landen, N.B. Meezan, and A.J. Mackinnon, Phys. Rev. E **91**, 021101 (2015).
[26] C.A. Thomas, E.M. Campbell, K.L. Baker, D.T. Casey, M. Hohenberger, A.L. Kritcher, B.K. Spears, S.F. Khan, R. Nora, D.T. Woods, J.L. Milovich, R.L. Berger, D. Strozzi, D.D. Ho, D. Clark, B. Bachmann, L.R. Benedetti, R. Bionta, P.M. Celliers, D.N. Fittinghoff, G. Grim, R. Hatarik, N. Izumi, G. Kyrala, T. Ma, M. Millot, S.R. Nagel, P.K. Patel, C. Yeamans, A. Nikroo, M. Tabak, M.G. Johnson, P.L. Volegov, and S.M. Finnegan, Phys. Plasmas **27**, 112708 (2020).
[27] K.L. Baker, C.A. Thomas, D.T. Casey, S. Khan, B.K. Spears, R. Nora, T. Woods, J.L. Milovich, R.L. Berger, D. Strozzi, D. Clark, M. Hohenberger, O.A. Hurricane, D.A. Callahan, O.L. Landen, B. Bachmann, R. Benedetti, R. Bionta, P.M. Celliers, D. Fittinghoff, C. Goyon, G. Grim, R. Hatarik, N. Izumi, M. Gatu Johnson, G. Kyrala, T. Ma, M. Millot, S.R. Nagel, A. Pak, P.K. Patel, D. Turnbull, P.L. Volegov, and C. Yeamans, Phys. Rev. Lett. **121**, 135001 (2018).
[28] D.T. Casey, C.A. Thomas, K.L. Baker, B.K. Spears, M. Hohenberger, S.F. Khan, R.C. Nora, C.R. Weber, D.T. Woods, O.A. Hurricane, D.A. Callahan, R.L. Berger, J.L. Milovich, P.K. Patel, T. Ma, A. Pak, L.R. Benedetti, M. Millot, C. Jarrott, O.L. Landen, R.M. Bionta, B.J. MacGowan, D.J. Strozzi, M. Stadermann, J. Biener, A. Nikroo, C.S. Goyon, N. Izumi, S.R. Nagel, B. Bachmann, P.L. Volegov, D.N. Fittinghoff, G.P. Grim, C.B. Yeamans, M. Gatu Johnson, J.A. Frenje, N. Rice, C. Kong, J. Crippen, J. Jaquez, K. Kangas, and C. Wild, Phys. Plasmas **25**, 056308 (2018).
[29] A.L. Kritcher, D.T. Casey, C.A. Thomas, A.B. Zylstra, M. Hohenberger, K. Baker, S. Le Pape, B. Bachmann, S. Bhandarkar, J. Biener, T. Braun, D. Clark, L. Divol, T. Döppner, D. Hinkel, C. Kong, D. Mariscal, M. Millot, J. Milovich, A. Nikroo, A. Pak, N. Rice, H. Robey, M. Stadermann, J. Sevier, D. Strozzi, C. Weber, C. Wild, B. Woodworth, J. Edwards, D.A. Callahan, and O.A. Hurricane, Phys. Plasmas **27**, 052710 (2020).
[30] A.B. Zylstra, S. MacLaren, S.A. Yi, J. Kline, D. Callahan, O. Hurricane, B. Bachmann, G. Kyrala, L. Masse, P. Patel, J.E. Ralph, J. Salmonson, P. Volegov, and C. Wilde, Phys. Plasmas **26**, 052707 (2019).
[31] A.L. Kritcher, A.B. Zylstra, D.A. Callahan, O.A. Hurricane, C. Weber, J. Ralph, D.T. Casey, A. Pak, K. Baker, B. Bachmann, S. Bhandarkar, J. Biener, R. Bionta, T. Braun, M. Bruhn, C. Choate, D. Clark, J.M. Di Nicola, L. Divol, T. Doeppner, V. Geppert-Kleinrath, S. Haan, J. Heebner, V. Hernandez, D. Hinkel, M. Hohenberger, H. Huang, C. Kong, S. Le Pape, D. Mariscal, E. Marley, L. Masse, K.D. Meaney, M. Millot, A. Moore, K. Newman, A. Nikroo, P. Patel, L. Pelz, N. Rice, H. Robey, J.S. Ross, M. Rubery, J. Salmonson, D. Schlossberg, S. Sepke, K. Sequoia, M. Stadermann, D. Strozzi, R. Tommasini, P. Volegov, C. Wild, S. Yang, C. Young, M.J. Edwards, O. Landen, R. Town, and M. Herrmann, Phys. Plasmas **28**, 072706 (2021).

[32] H.F. Robey, L. Berzak Hopkins, J.L. Milovich, and N.B. Meezan, Phys. Plasmas **25**, 012711 (2018).
[33] D.S. Clark, D.T. Casey, C.R. Weber, O.S. Jones, K.L. Baker, E.L. Dewald, L. Divol, A. Do, A.L. Kritcher, O.L. Landen, M. Millot, J.L. Milovich, V.A. Smalyuk, D.J. Strozzi, A.E. Pak, R. Tommasini, and M.J. Edwards, Phys. Plasmas **29**, 052710 (2022).
[34] A. Lees, R. Betti, J.P. Knauer, V. Gopalaswamy, D. Patel, K.M. Woo, K.S. Anderson, E.M. Campbell, D. Cao, J. Carroll-Nellenback, R. Epstein, C. Forrest, V.N. Goncharov, D.R. Harding, S.X. Hu, I.V. Igumenshchev, R.T. Janezic, O.M. Mannion, P.B. Radha, S.P. Regan, A. Shvydky, R.C. Shah, W.T. Shmayda, C. Stoeckl, W. Theobald, and C. Thomas, Phys. Rev. Lett. **127**, 105001 (2021).
[35] D.S. Clark, C.R. Weber, J.L. Milovich, A.E. Pak, D.T. Casey, B.A. Hammel, D.D. Ho, O.S. Jones, J.M. Koning, A.L. Kritcher, M.M. Marinak, L.P. Masse, D.H. Munro, M.V. Patel, P.K. Patel, H.F. Robey, C.R. Schroeder, S.M. Sepke, and M.J. Edwards, Phys. Plasmas **26**, 050601 (2019).
[36] A.B. Zylstra, D.T. Casey, A. Kritcher, L. Pickworth, B. Bachmann, K. Baker, J. Biener, T. Braun, D. Clark, V. Geppert-Kleinrath, M. Hohenberger, C. Kong, S. Le Pape, A. Nikroo, N. Rice, M. Rubery, M. Stadermann, D. Strozzi, C. Thomas, P. Volegov, C. Weber, C. Wild, C. Wilde, D.A. Callahan, and O.A. Hurricane, Phys. Plasmas **27**, 092709 (2020).
[37] T. Chen and C. Guestrin, in *Proc. 22nd ACM SIGKDD Int. Conf. Knowl. Discov. Data Min.* (Association for Computing Machinery, New York, NY, USA, 2016), pp. 785–794.
[38] T. Chen and T. He, in *NIPS 2014 Workshop High-Energy Phys. Mach. Learn.* (PMLR, 2015), pp. 69–80.
[39] M.G. Fernández-Godino, M.J. Grosskopf, J.B. Nakhleh, B.M. Wilson, J. Kline, and G. Srinivasan, ArXiv201015208 Phys. Stat (2020).
[40] O.A. Hurricane, A. Kritcher, D.A. Callahan, O. Landen, P.K. Patel, P.T. Springer, D.T. Casey, E.L. Dewald, T.R. Dittrich, T. Döppner, D.E. Hinkel, L.F. Berzak Hopkins, J. Kline, S. Le Pape, T. Ma, A.G. MacPhee, A. Moore, A. Pak, H.-S. Park, J. Ralph, J.D. Salmonson, and K. Widmann, Phys. Plasmas **24**, 092706 (2017).
[41] P. Michel, L. Divol, E.A. Williams, S. Weber, C.A. Thomas, D.A. Callahan, S.W. Haan, J.D. Salmonson, S. Dixit, D.E. Hinkel, M.J. Edwards, B.J. MacGowan, J.D. Lindl, S.H. Glenzer, and L.J. Suter, Phys. Rev. Lett. **102**, 025004 (2009).
[42] J.R. Rygg, O.S. Jones, J.E. Field, M.A. Barrios, L.R. Benedetti, G.W. Collins, D.C. Eder, M.J. Edwards, J.L. Kline, J.J. Kroll, O.L. Landen, T. Ma, A. Pak, J.L. Peterson, K. Raman, R.P.J. Town, and D.K. Bradley, Phys. Rev. Lett. **112**, 195001 (2014).
[43] K.L. Baker, C.A. Thomas, D.T. Casey, M. Hohenberger, S. Khan, B.K. Spears, O.L. Landen, R. Nora, D.T. Woods, J.L. Milovich, R.L. Berger, D. Strozzi, C. Weber, D. Clark, O.A. Hurricane, D.A. Callahan, A.L. Kritcher, B. Bachmann, L.R. Benedetti, R. Bionta, P.M. Celliers, D. Fittinghoff, C. Goyon, R. Hatarik, N. Izumi, M. Gatu Johnson, G. Kyrala, T. Ma, K. Meaney, M. Millot, S.R. Nagel, P.K. Patel, D. Turnbull, P.L. Volegov, C. Yeamans, and C. Wilde, Phys. Rev. E **102**, 023210 (2020).
[44] D.A. Callahan, O.A. Hurricane, A.L. Kritcher, D.T. Casey, D.E. Hinkel, Y.P. Opachich, H.F. Robey, M.D. Rosen, J.S. Ross, M.S. Rubery, C.V. Young, and A.B. Zylstra, Phys. Plasmas **27**, 072704 (2020).
[45] M.M. Pokornik, S.F. Khan, A.D. Maris, K.D. Humbird, J.L. Peterson, and J.A. Gaffney, J. Plasma Phys. **Manuscript in Preparation**, (n.d.).

[46] M.M. Marinak, R.E. Tipton, O.L. Landen, T.J. Murphy, P. Amendt, S.W. Haan, S.P. Hatchett, C.J. Keane, R. McEachern, and R. Wallace, Phys. Plasmas **3**, 2070 (1996).
[47] H.F. Robey, P.M. Celliers, J.L. Kline, A.J. Mackinnon, T.R. Boehly, O.L. Landen, J.H. Eggert, D. Hicks, S. Le Pape, D.R. Farley, M.W. Bowers, K.G. Krauter, D.H. Munro, O.S. Jones, J.L. Milovich, D. Clark, B.K. Spears, R.P.J. Town, S.W. Haan, S. Dixit, M.B. Schneider, E.L. Dewald, K. Widmann, J.D. Moody, T.D. Döppner, H.B. Radousky, A. Nikroo, J.J. Kroll, A.V. Hamza, J.B. Horner, S.D. Bhandarkar, E. Dzenitis, E. Alger, E. Giraldez, C. Castro, K. Moreno, C. Haynam, K.N. LaFortune, C. Widmayer, M. Shaw, K. Jancaitis, T. Parham, D.M. Holunga, C.F. Walters, B. Haid, T. Malsbury, D. Trummer, K.R. Coffee, B. Burr, L.V. Berzins, C. Choate, S.J. Brereton, S. Azevedo, H. Chandrasekaran, S. Glenzer, J.A. Caggiano, J.P. Knauer, J.A. Frenje, D.T. Casey, M. Gatu Johnson, F.H. Séguin, B.K. Young, M.J. Edwards, B.M. Van Wonterghem, J. Kilkenny, B.J. MacGowan, J. Atherton, J.D. Lindl, D.D. Meyerhofer, and E. Moses, Phys. Rev. Lett. **108**, 215004 (2012).
[48] S.W. Haan, P.A. Amendt, T.R. Dittrich, S.P. Hatchett, M.C. Herrmann, O.A. Hurricane, M.M. Marinak, D. Munro, S.M. Pollaine, G.A. Strobel, and L.J. Suter, Fusion Sci. Technol. **45**, 69 (2004).
[49] T.R. Dittrich, O.A. Hurricane, L.F. Berzak-Hopkins, D.A. Callahan, D.T. Casey, D. Clark, E.L. Dewald, T. Doeppner, S.W. Haan, B.A. Hammel, J.A. Harte, D.E. Hinkel, B.J. Kozioziemski, A.L. Kritcher, T. Ma, A. Nikroo, A.E. Pak, T.G. Parham, H.-S. Park, P.K. Patel, B.A. Remington, J.D. Salmonson, P.T. Springer, C.R. Weber, G.B. Zimmerman, and J.L. Kline, J. Phys. Conf. Ser. **717**, 012013 (2016).
[50] L.A. Pickworth, B.A. Hammel, V.A. Smalyuk, H.F. Robey, R. Tommasini, L.R. Benedetti, L. Berzak Hopkins, D.K. Bradley, M. Dayton, S. Felker, J.E. Field, S.W. Haan, B. Haid, R. Hatarik, E. Hartouni, D. Holunga, M. Hoppe, N. Izumi, S. Johnson, S. Khan, T. Kohut, B. Lahmann, O.L. Landen, S. LePape, A.G. MacPhee, E. Marley, N.B. Meezan, J. Milovich, S.R. Nagel, A. Nikroo, A.E. Pak, R. Petrasso, B.A. Remington, N.G. Rice, H.A. Scott, P.T. Springer, M. Stadermann, C. Walters, K. Widmann, and W.W. Hsing, Phys. Plasmas **25**, 082705 (2018).
[51] B.J. Kozioziemski, E.R. Mapoles, J.D. Sater, A.A. Chernov, J.D. Moody, J.B. Lugten, and M.A. Johnson, Fusion Sci. Technol. (2017).

Appendix

A: Hyperparameters

The hyperparameters used in these models are as follows:

- GBDT Booster: DART
- Evaluation Metric: Mean Absolute Error
- Gamma: 0.0005
- Learning rate: 0.01
- Max depth: 4
- Min child weight:2
- Number of parallel trees: 40
- Objective function: Squared Error (regression)
- Alpha: 0.01

- Lambda: 0.005
- Tree method: auto
- Subsample: 0.4
- Skip drop: 0.5
- Rate drop: 0.2
- Column sample by tree: 0.45
- Column sample by level: 0.45

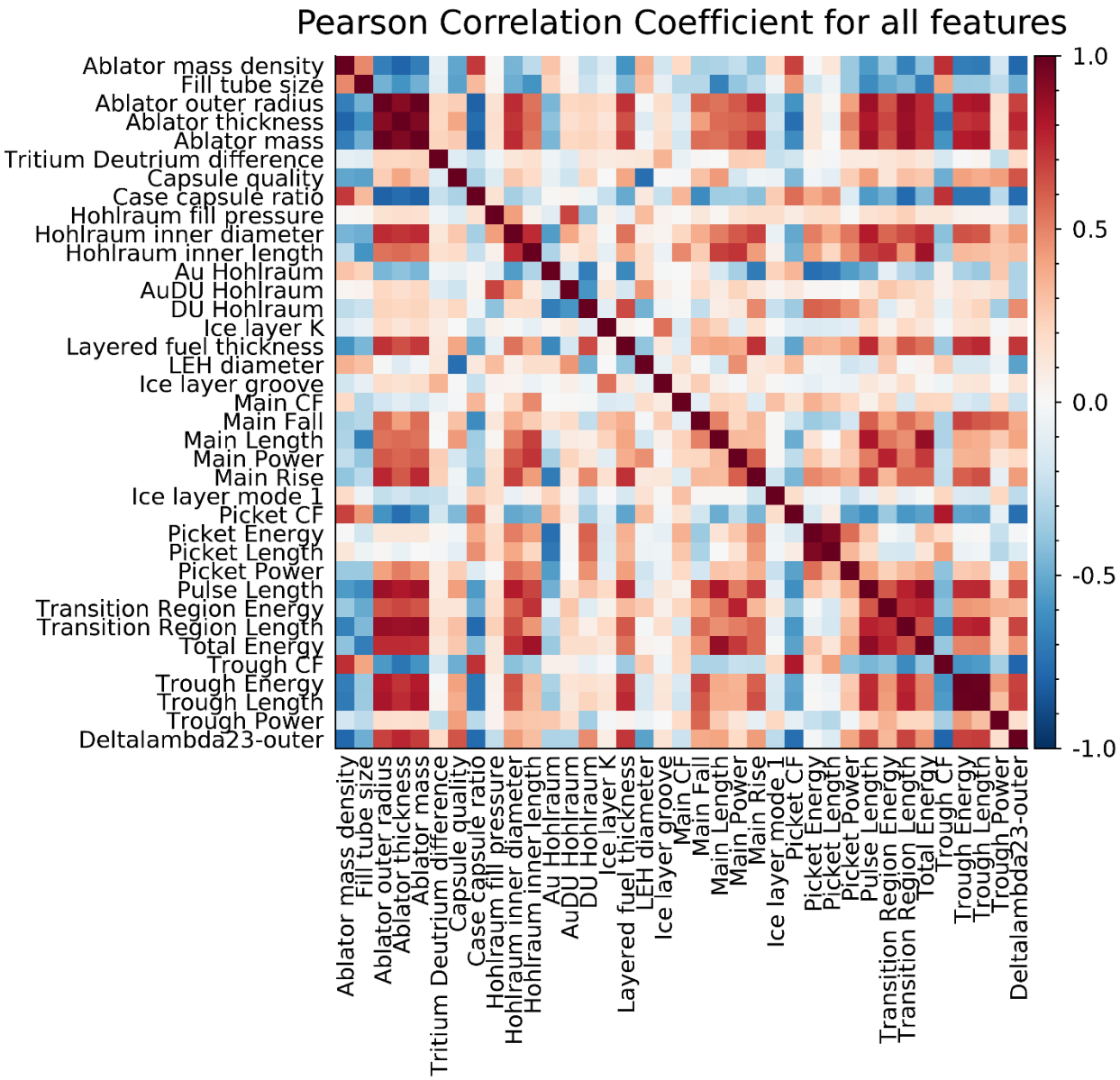

- Column sample by node: 0.45

B: Correlation Matrix

Figure 10: Correlation matrix of the 37 input variables and 1 label (Yn (13-15MeV) to the machine learning model calculated with the Pearson Correlation coefficient.